3. Distribution of geochemical anomaly values

A threshold value is determined, taking into consideration of a percentile, mean and standard deviation values, a break point and a natural gap of a probability plot in Fig. II-2-5-1. Table II-2-5-4 shows the threshold of each element.

Fig. II-2-5-2 to -10 show the anomaly values distribution charts of each element. Fig II-2-5-2 to -5 also show the charts of the MMI technique, in order to compare with the results of both methods.

Table II-2-5-4 Division into geochemical anomaly levels of soil samples in the Mae Kanai Area

Element	Unit	Background	High anomaly1	High anomaly2
Au	ppb	3.1	10	
Ag	ppm	0.30	0.7	
As	ppm	141	289	
Ba	ppm	973	1,602	
Cd	ppm	0.27	0.9	
Cu	ppm	186	355	
Fe	%	10.94		
Hg	ppb	156	361	
Mg	%	0.17	0.33	
Mn	ppm	4,541		
Pb	ppm	663	1,164	
Sb	ppm	31	65	
Zn	ppm	227	786	

[Zn] The north-northwest trending Zn anomaly zone extends from the middle of Line C to the middle of Line F. The high anomaly values in the anomaly zone center on three sub-areas: the area around the intersection of Line C and the main road; the area around the intersection of Line F and the branch road to Ban Sam Lung; the area around the middle of LineF.

[Pb] The north-northwest trending Pb anomaly zone extends from the middle of Line D to the middle of Line G ranging from 100 to 250 meters wide. The shape of this zone is almost similar to that of Zn, but anomalous zone does not continue to the north of Line D.

[Cu] The north-northwest trending Cu anomaly zone extends from the middle of Line C to the middle of Line G. The shape is almost similar to that of Pb. The high values also overlap with the Silurian-Devonian sandstone in the northeast of the survey area. These values may reflect the high background of its sandstone area.

[Cd] The Cd values are low as a whole, and no anomaly zone is detected.

[Ag] The Ag anomaly values center on the area around the intersection of Line D and the branch road to Ban Sam Lung, and the middle of Line F. Some high values are distributed at the gossan zone south of Ban Sam Lung.

[As] The anomaly values of As almost overlap with those of Ag, but some anomaly values scatter on the middle of Line I.

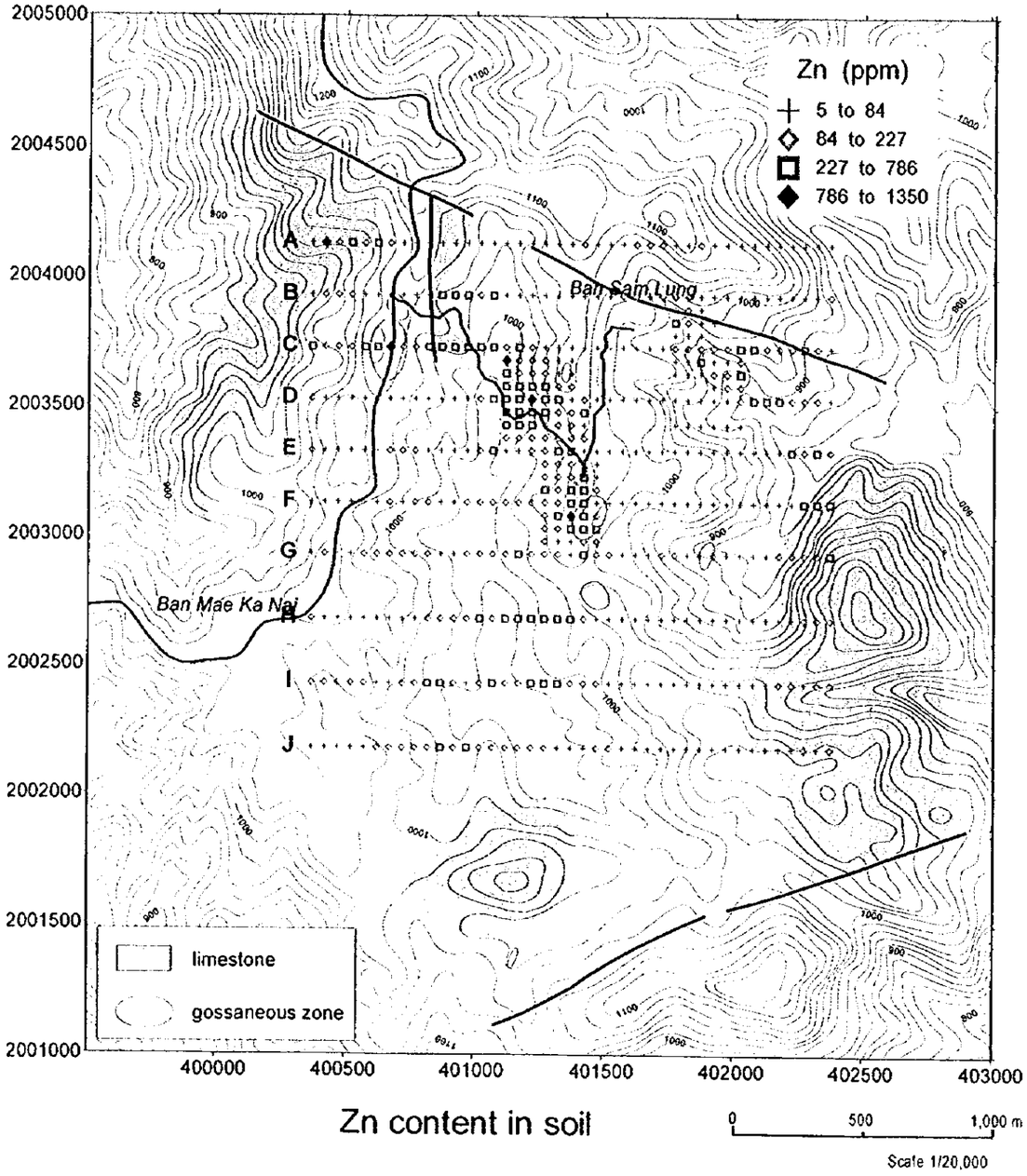

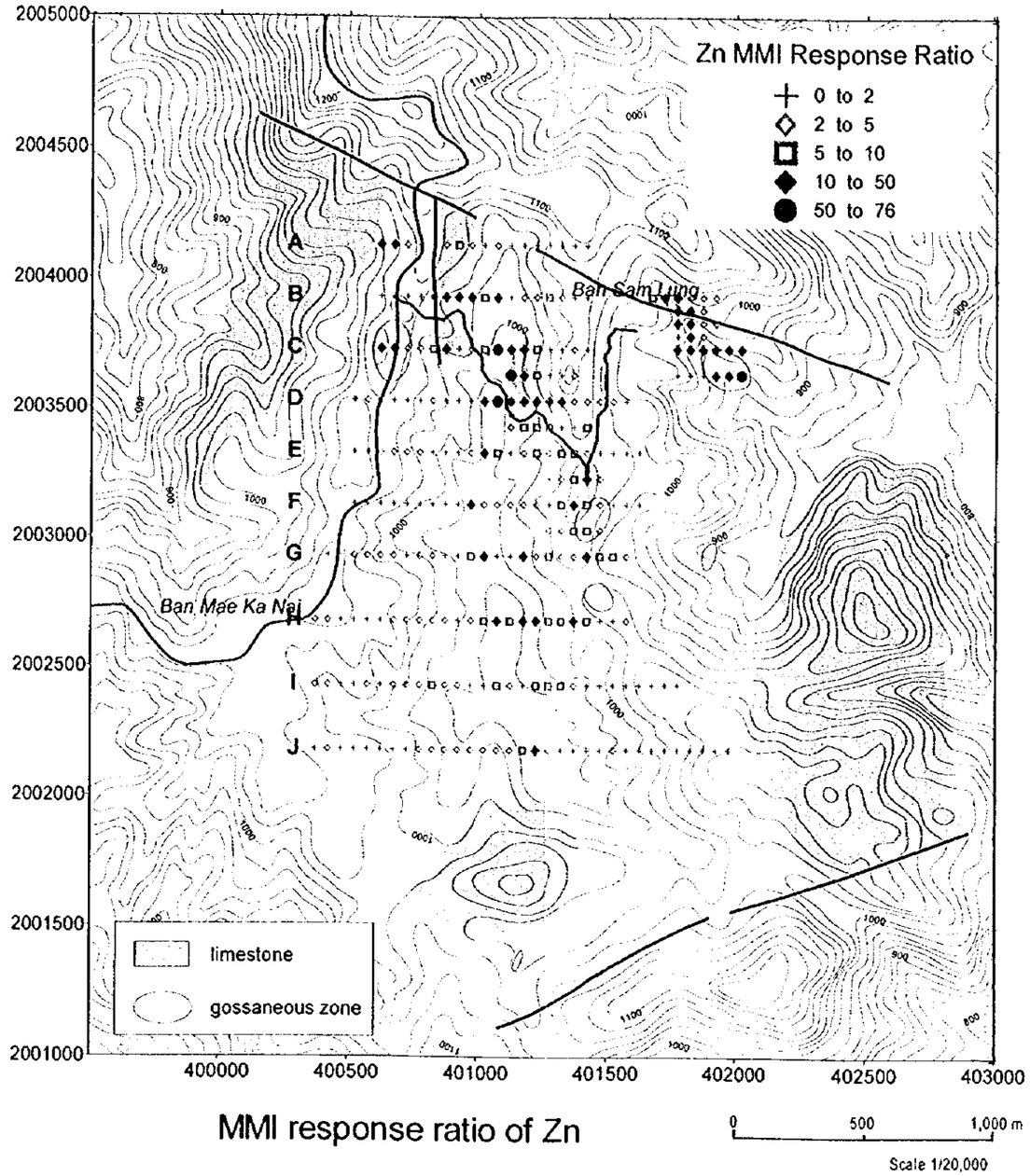

Fig. II-2-5-2 Zn content in soil and Zn MMI Response Ratio of the Mae Kanai Area

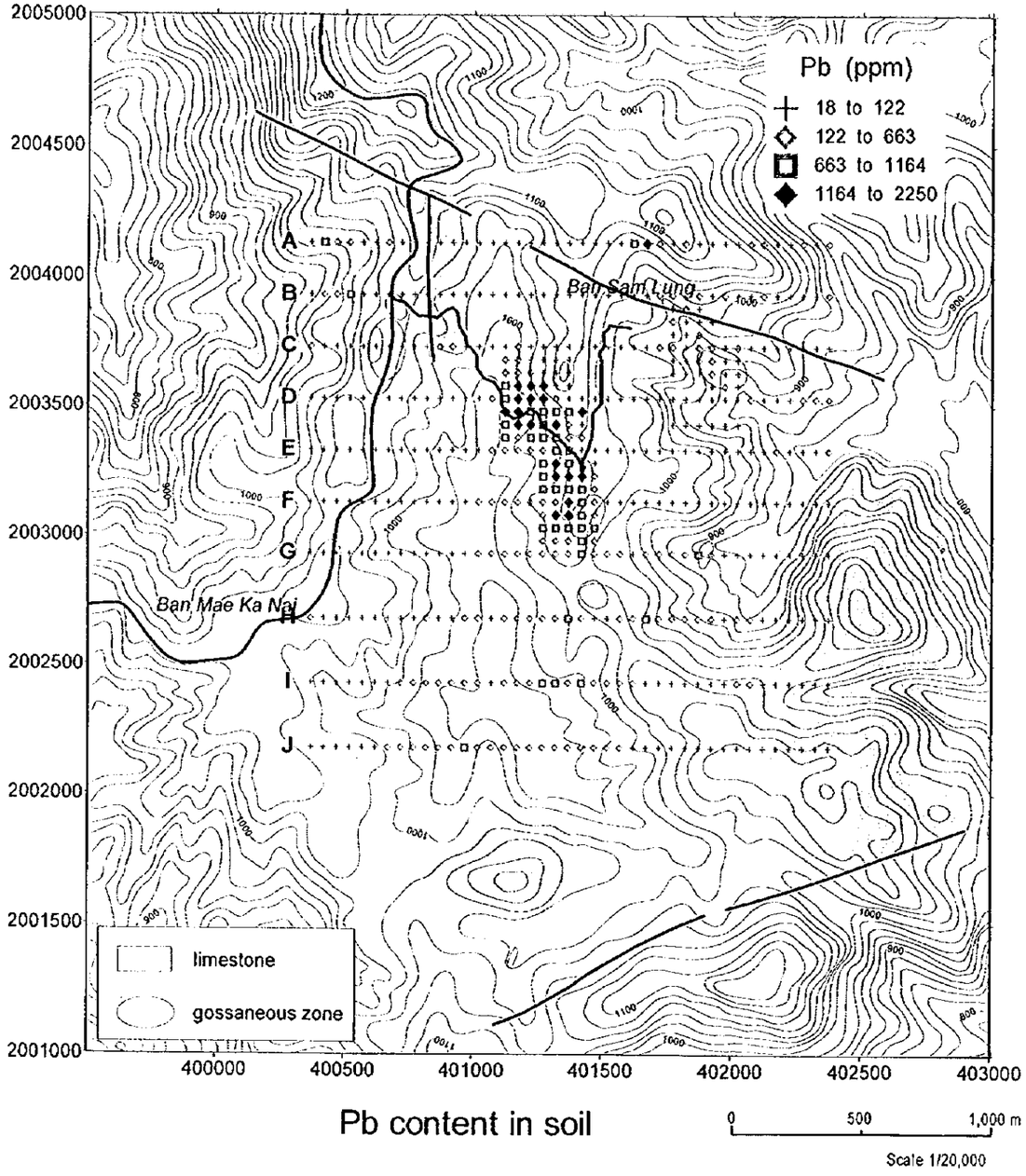

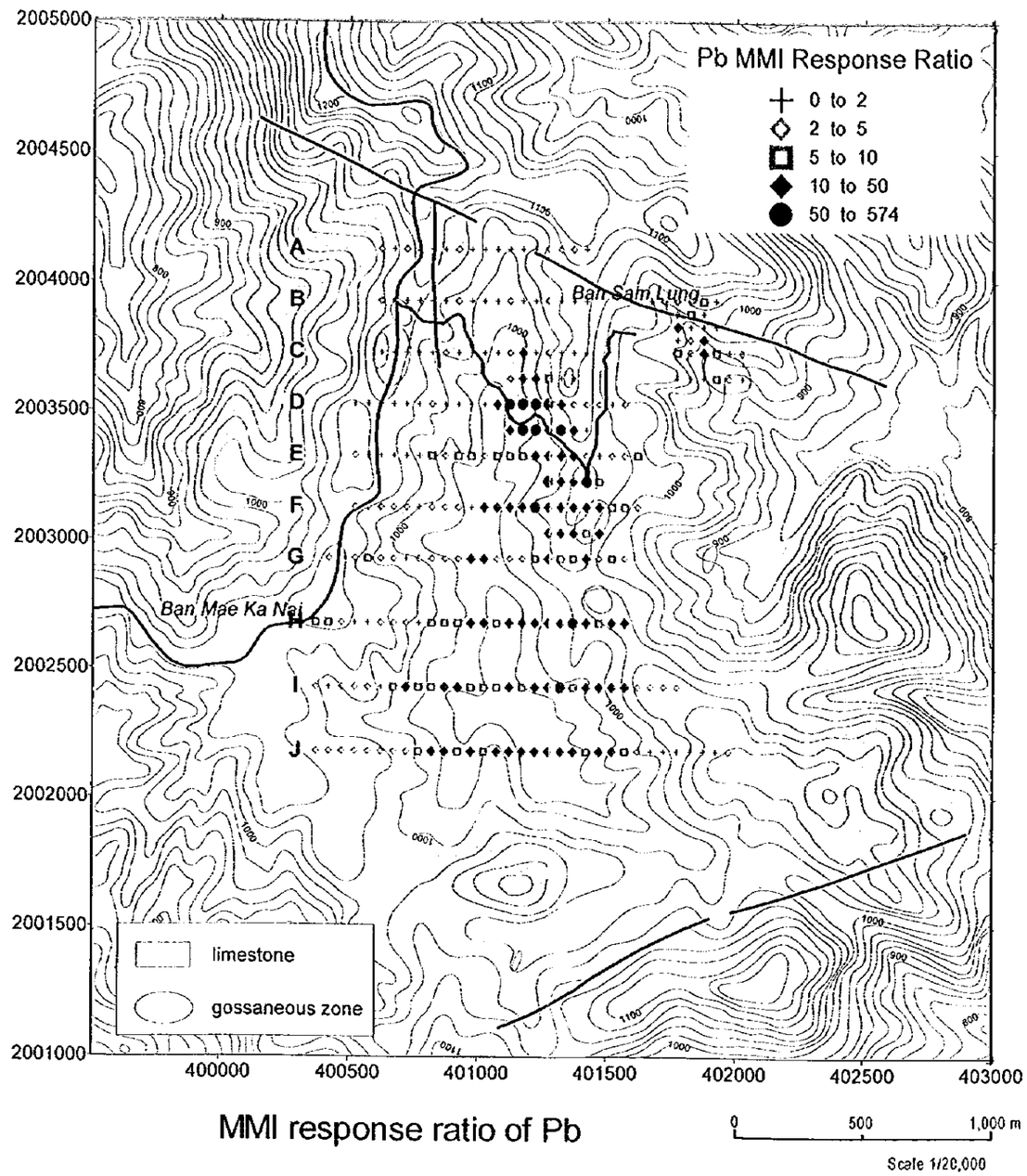

Fig. II-2-5-3 Pb content in soil and Pb MMI Response Ratio of the Mae Kanai Area

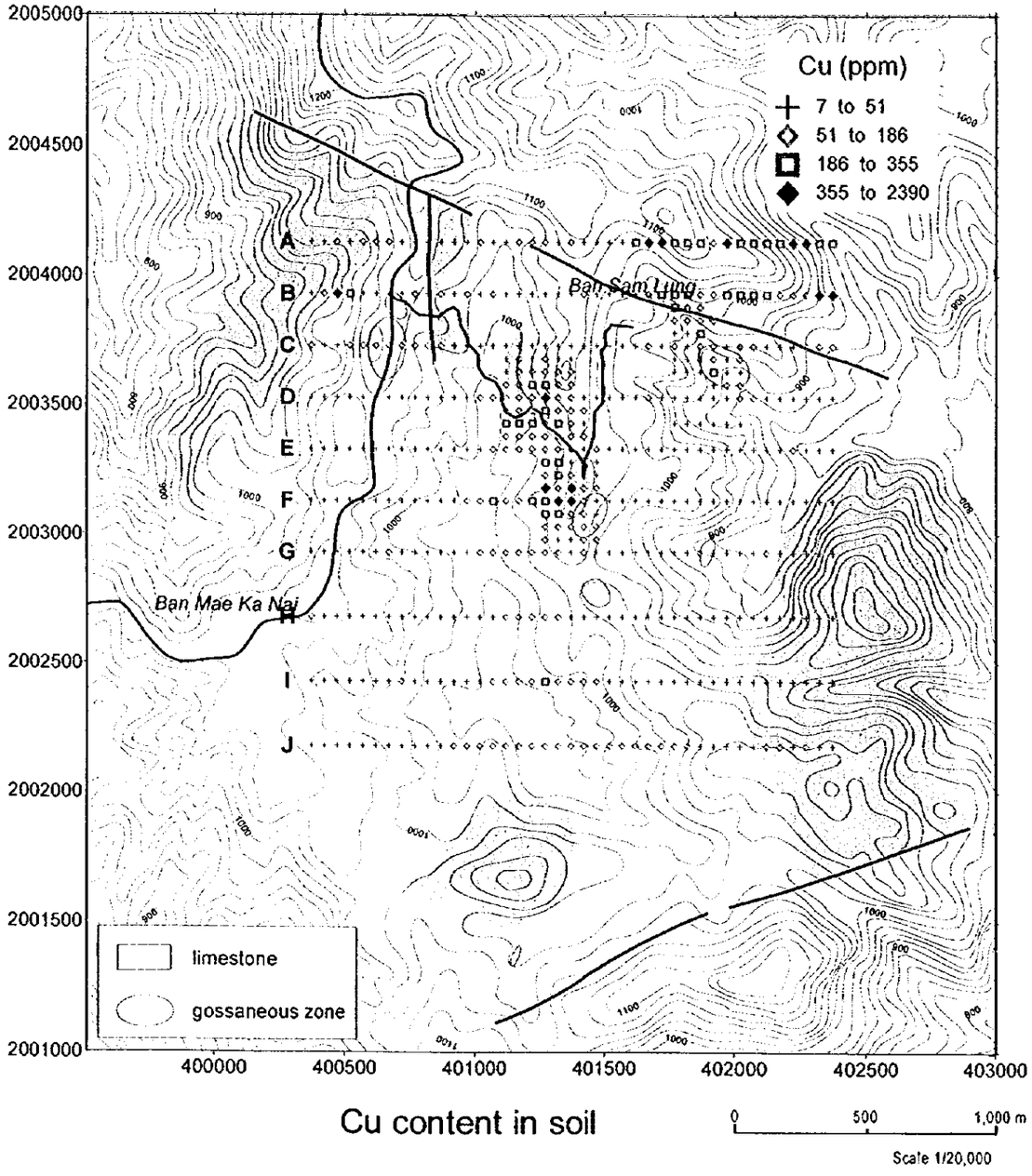

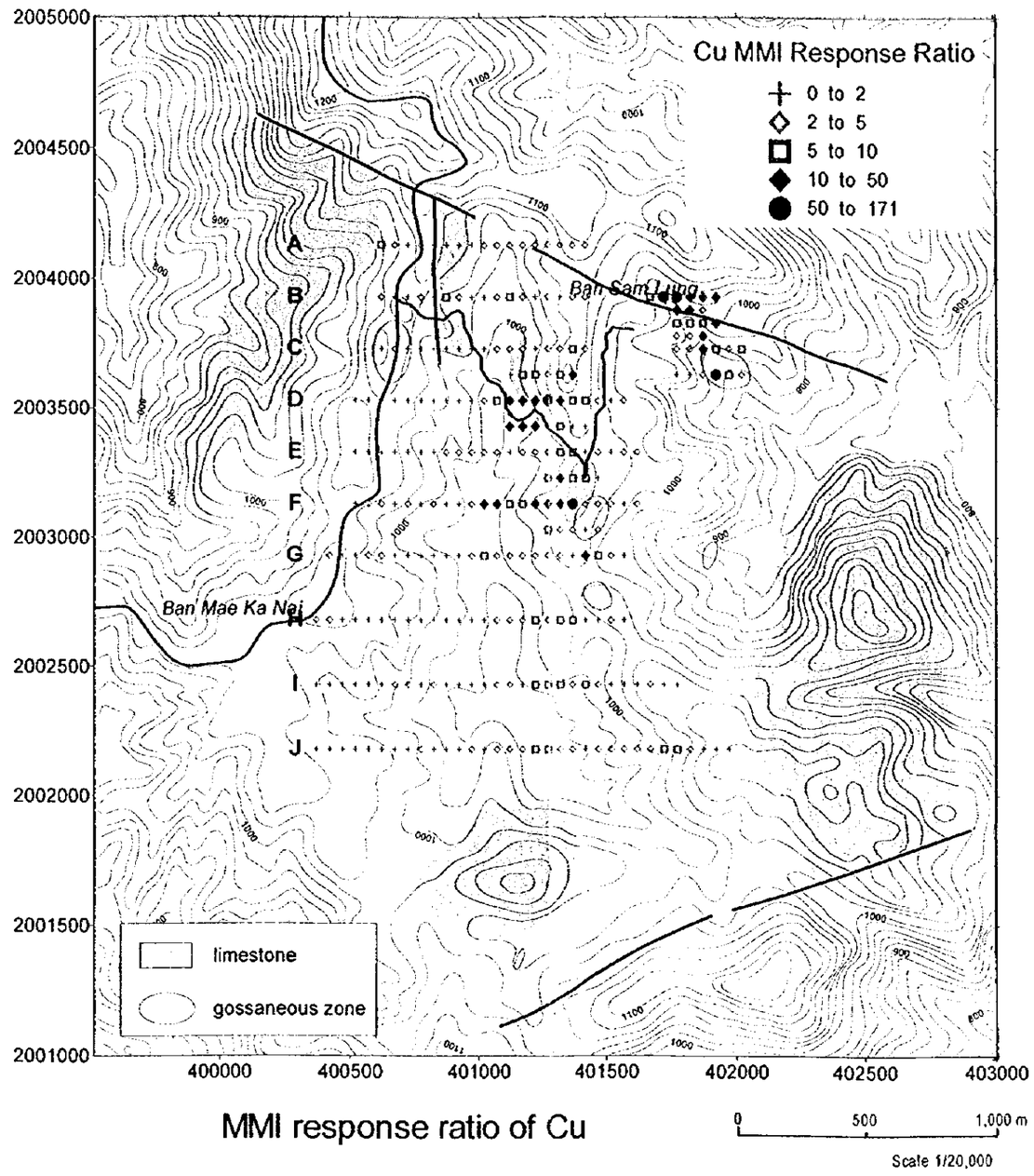

Fig. II-2-5-4 Cu content in soil and Cu MMI Response Ratio of the Mae Kanai Area

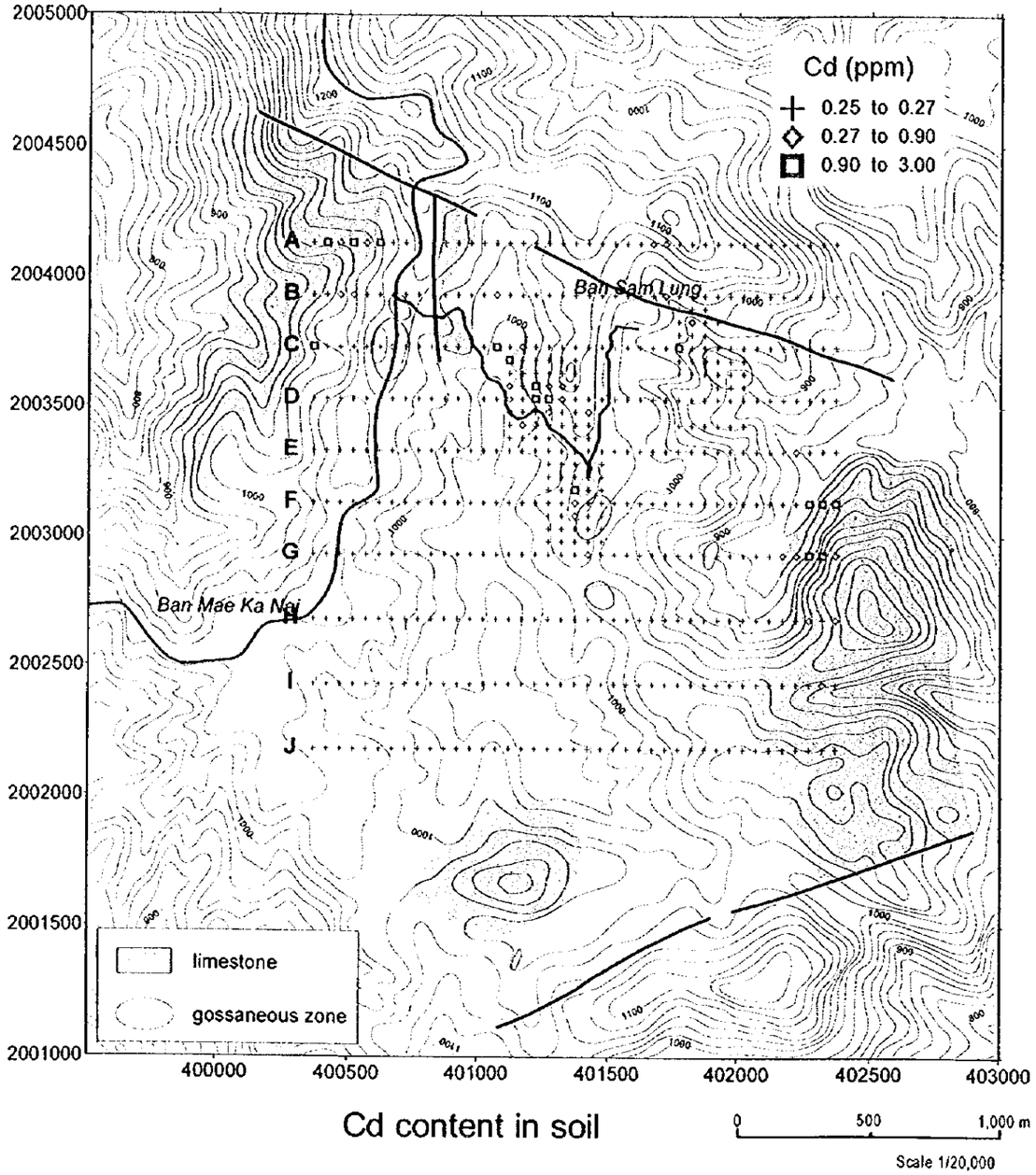

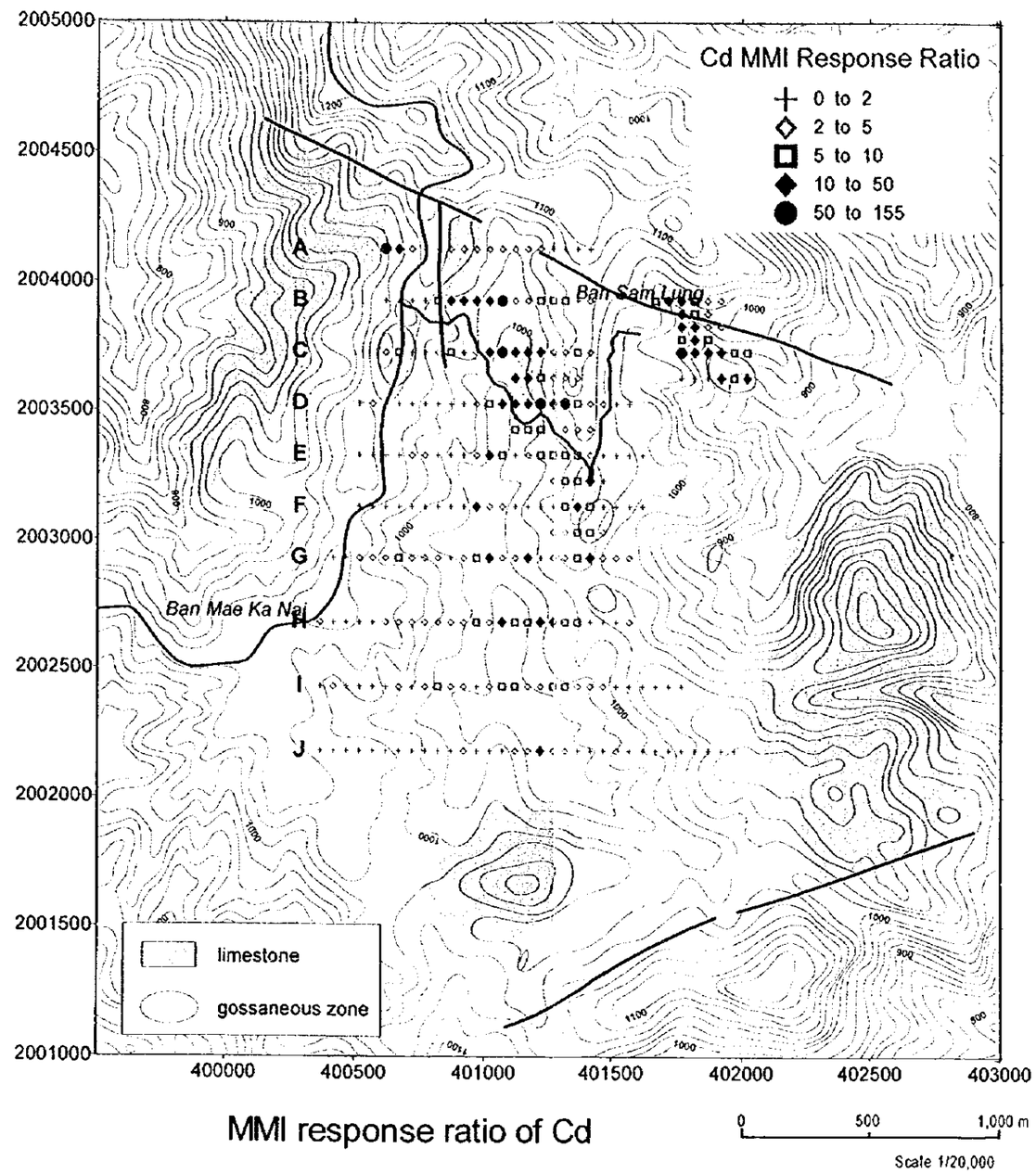

Fig. II-2-5-5 Cd content in soil and Cd MMI Response Ratio of the Mae Kanai Area

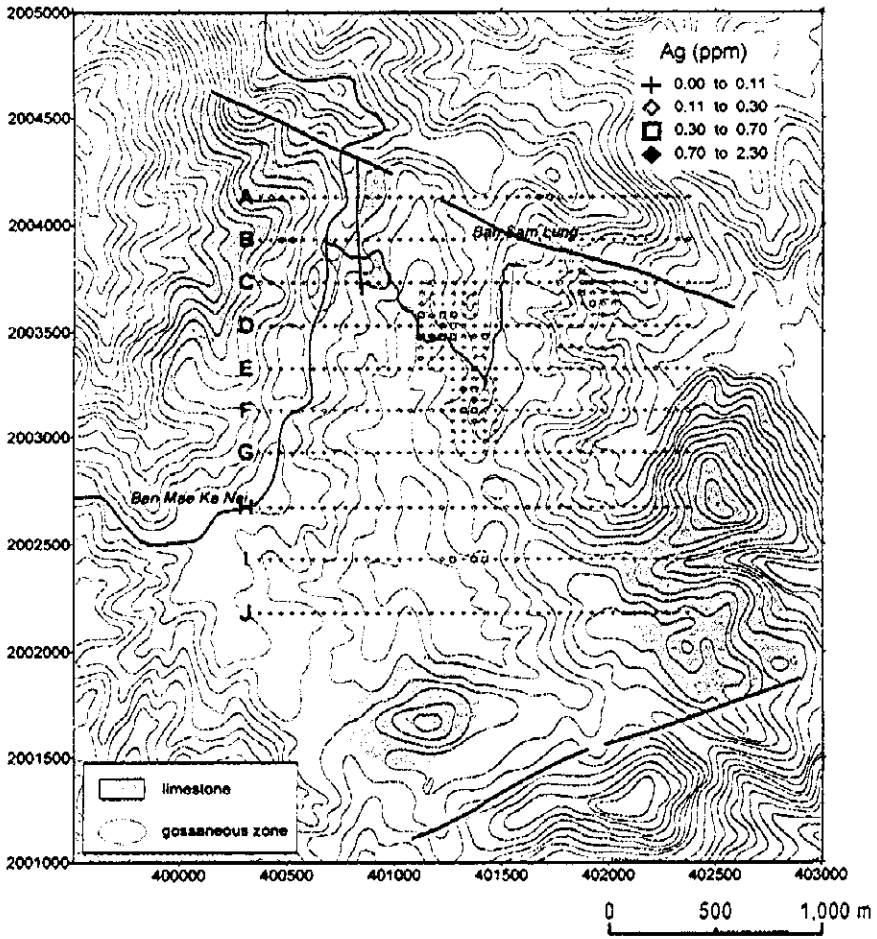

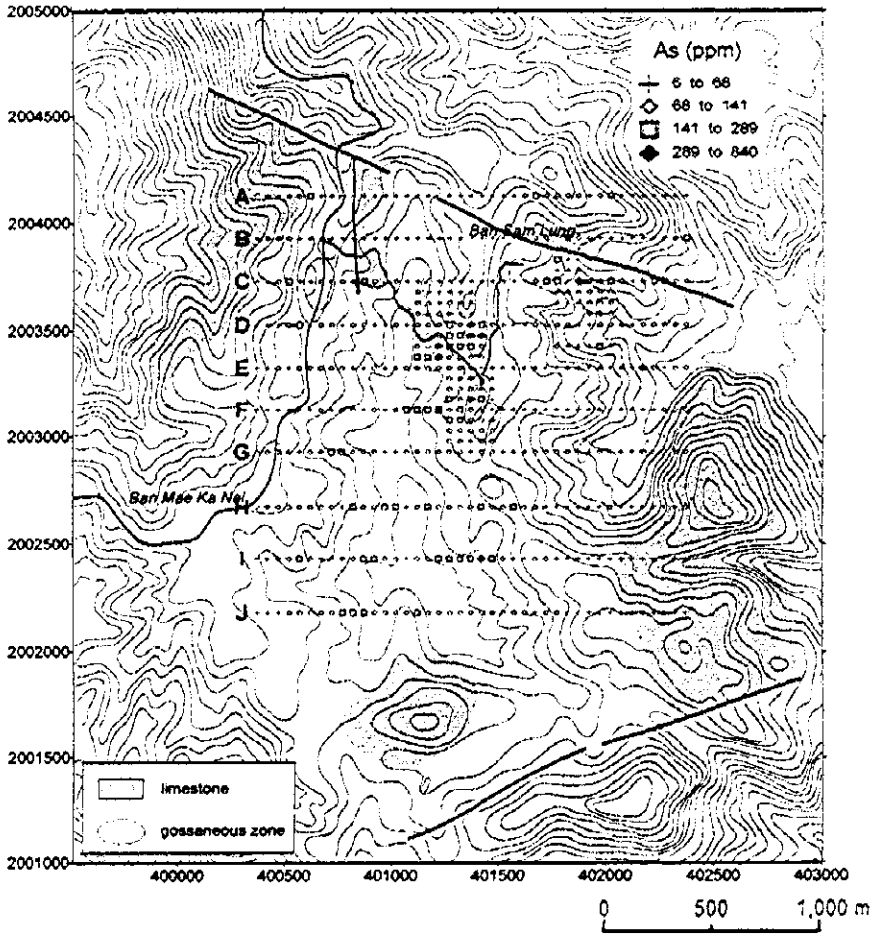

Fig. II-2-5-6 Geochemical map of Ag and As content in soil of the Mae Kanai Area

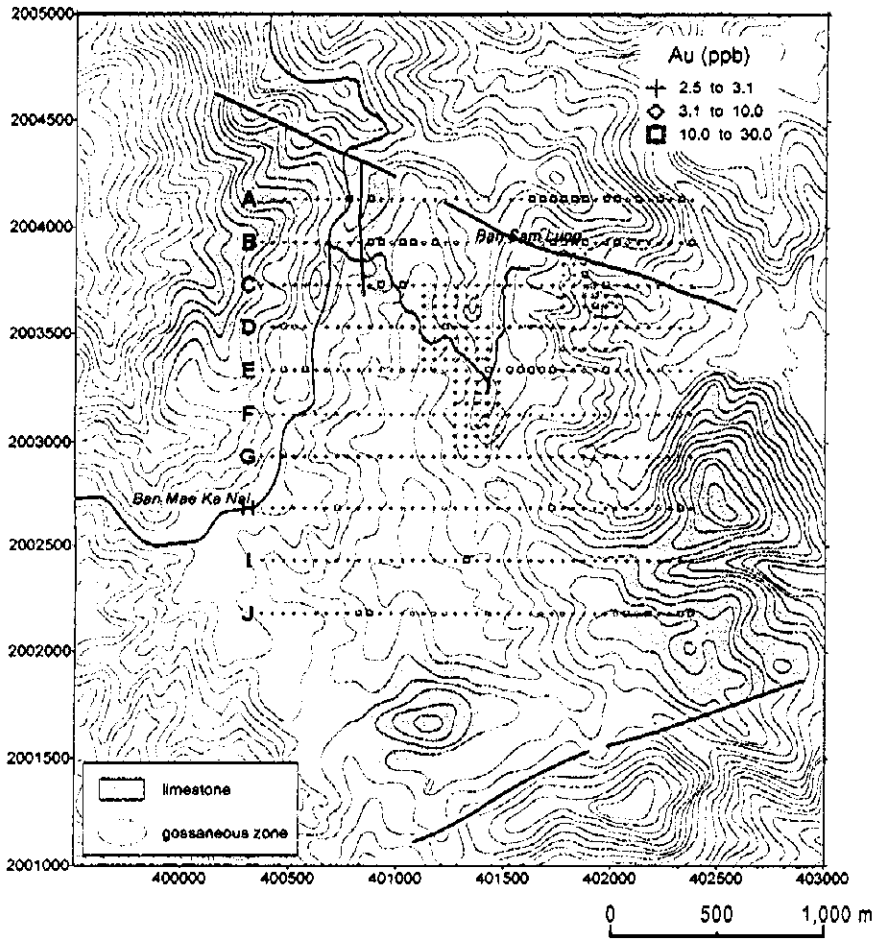

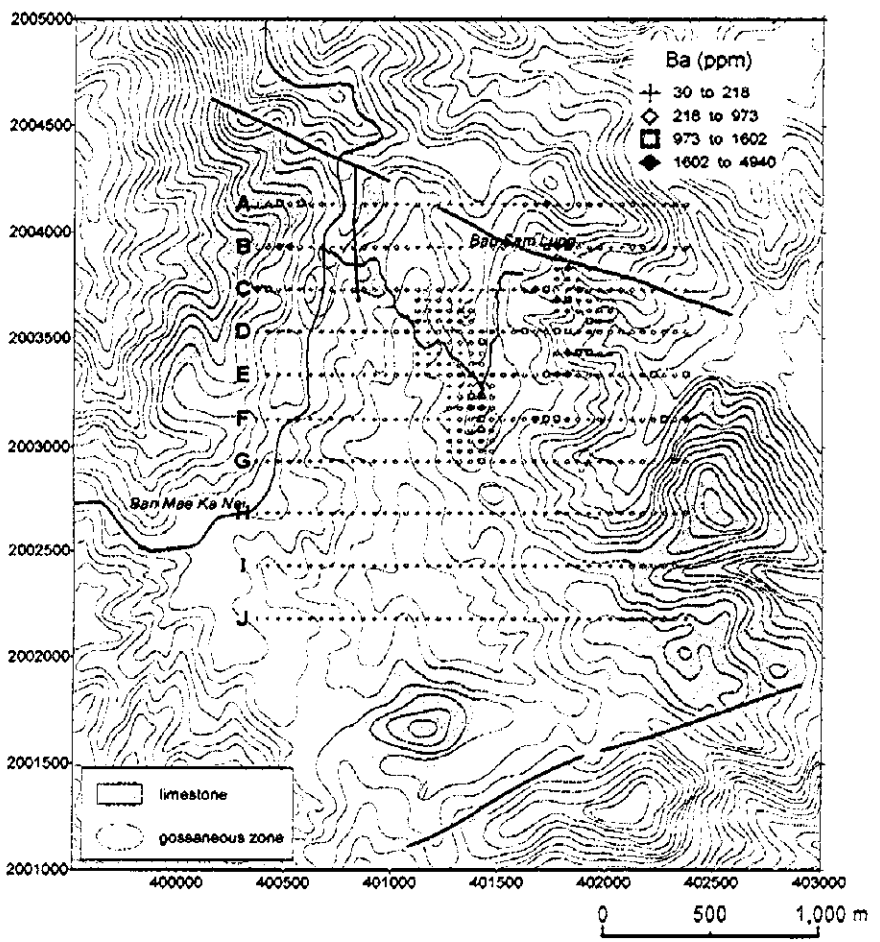

Fig. II-2-5-7 Geochemical map of Au and Ba content in soil of the Mae Kanai Area

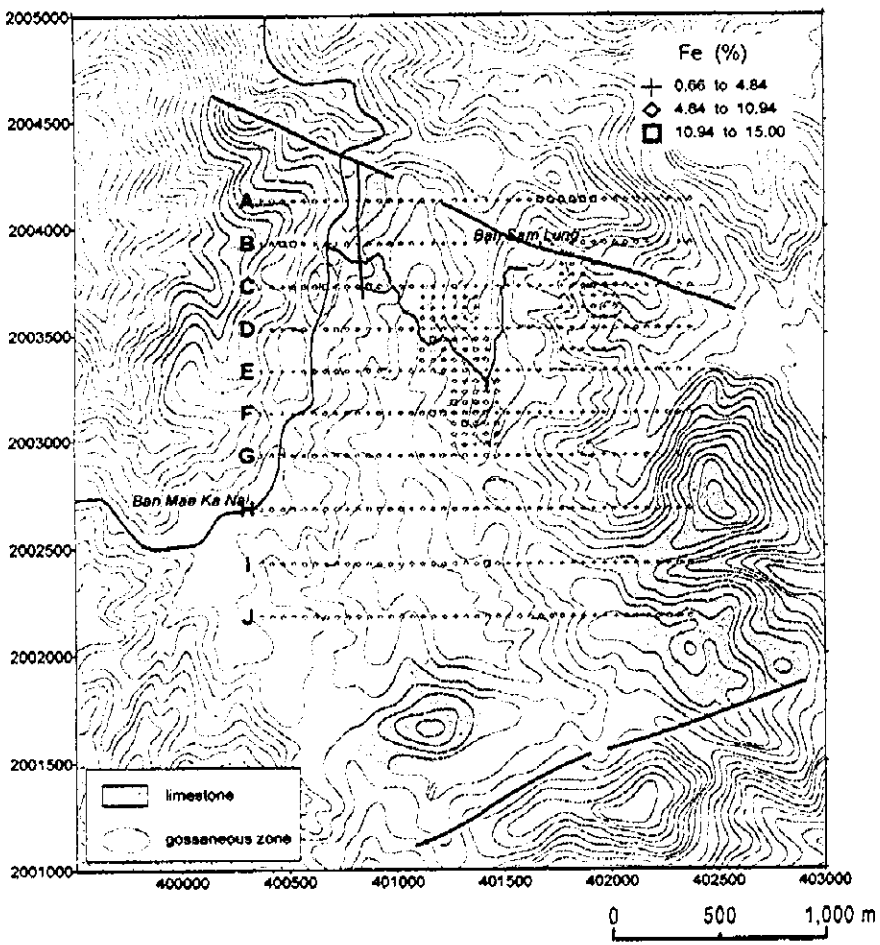

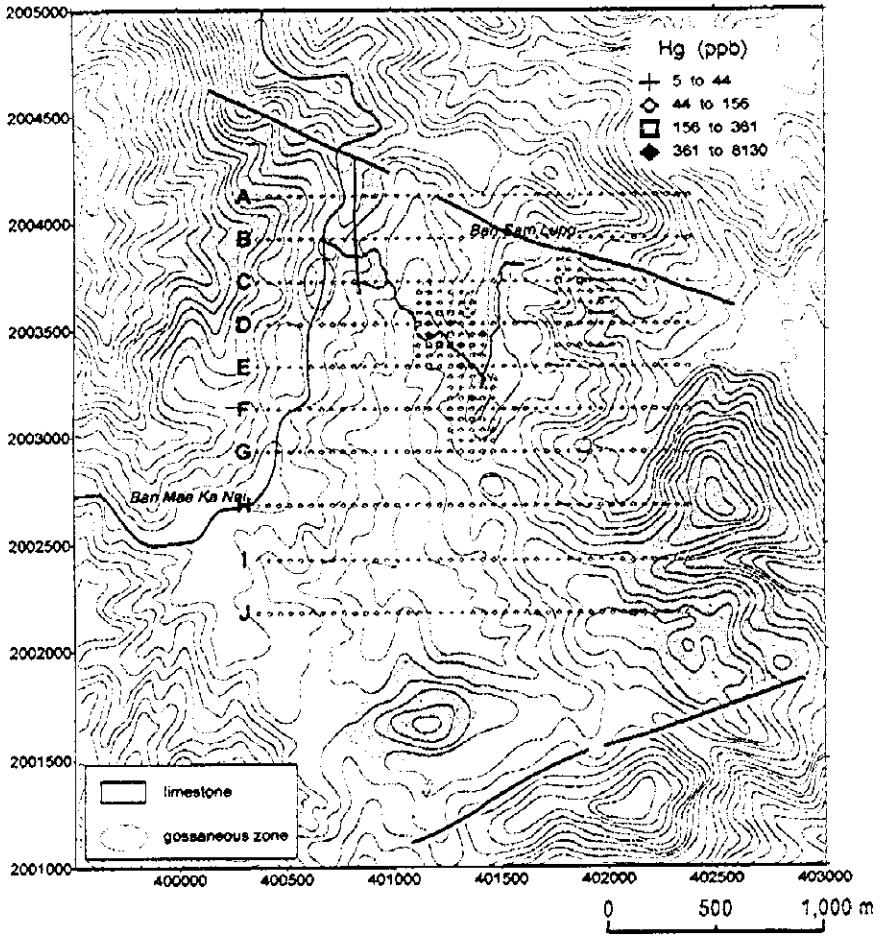

Fig. II-2-5-8 Geochemical map of Fe and Mg content in soil of the Mae Kanai Area

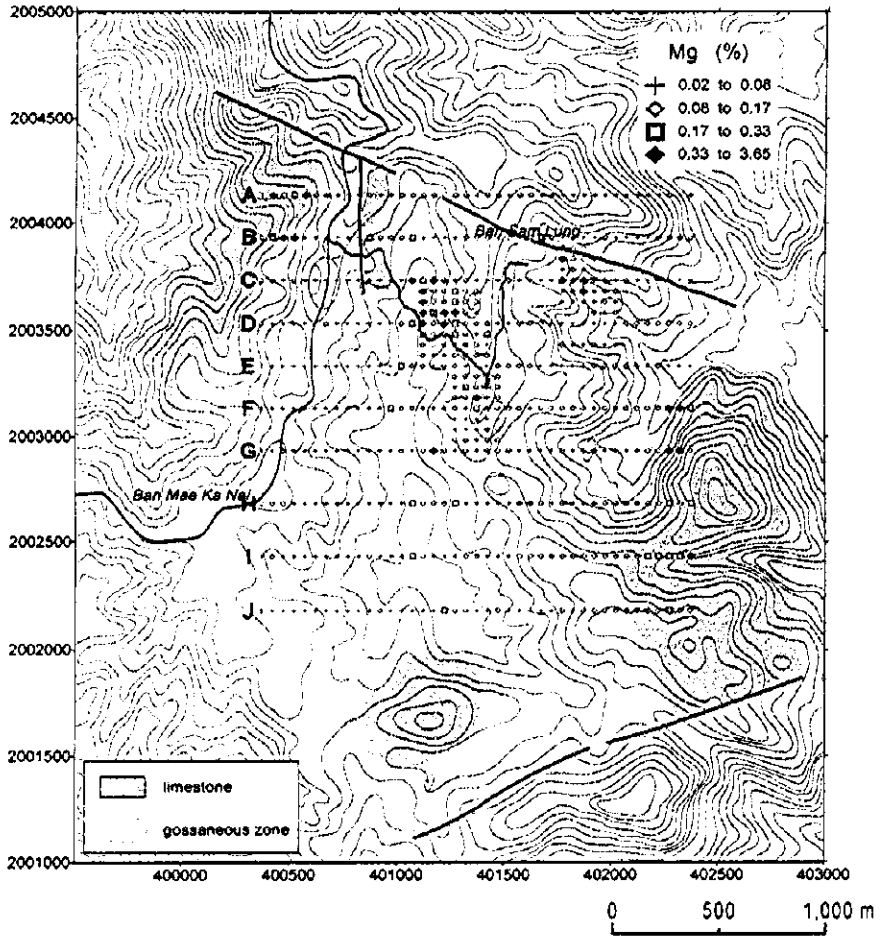

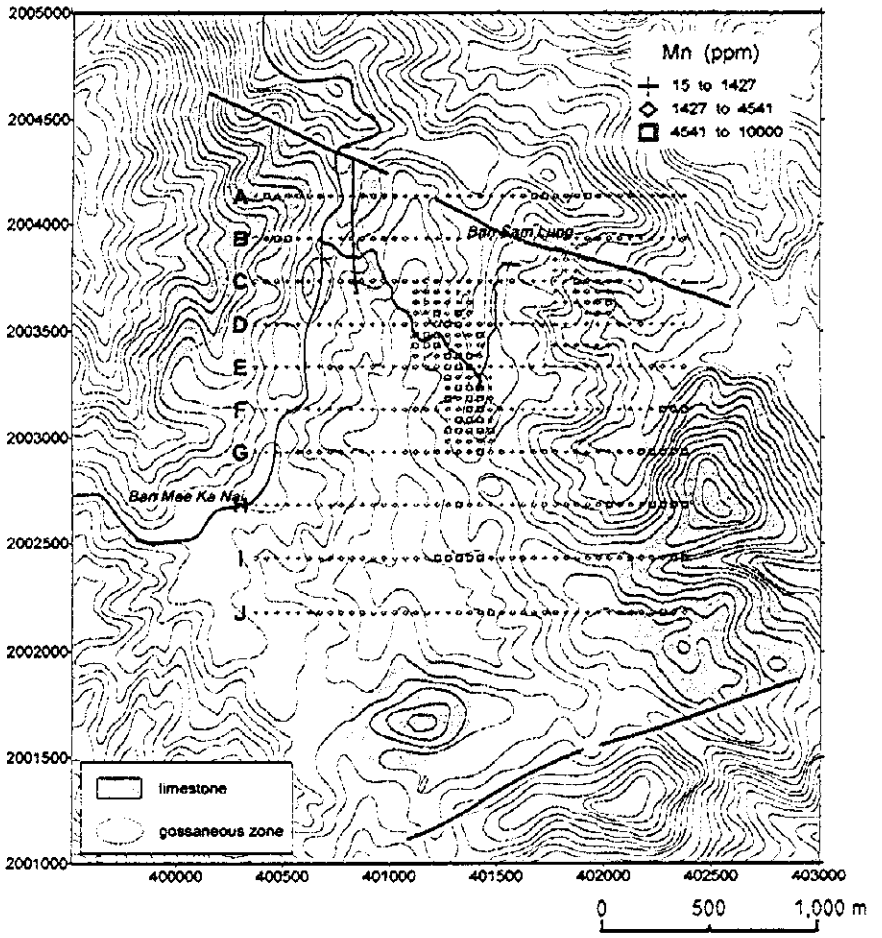

Fig. II-2-5-9 Geochemical map of Mg and Mn content in soil of the Mae Kanai Area

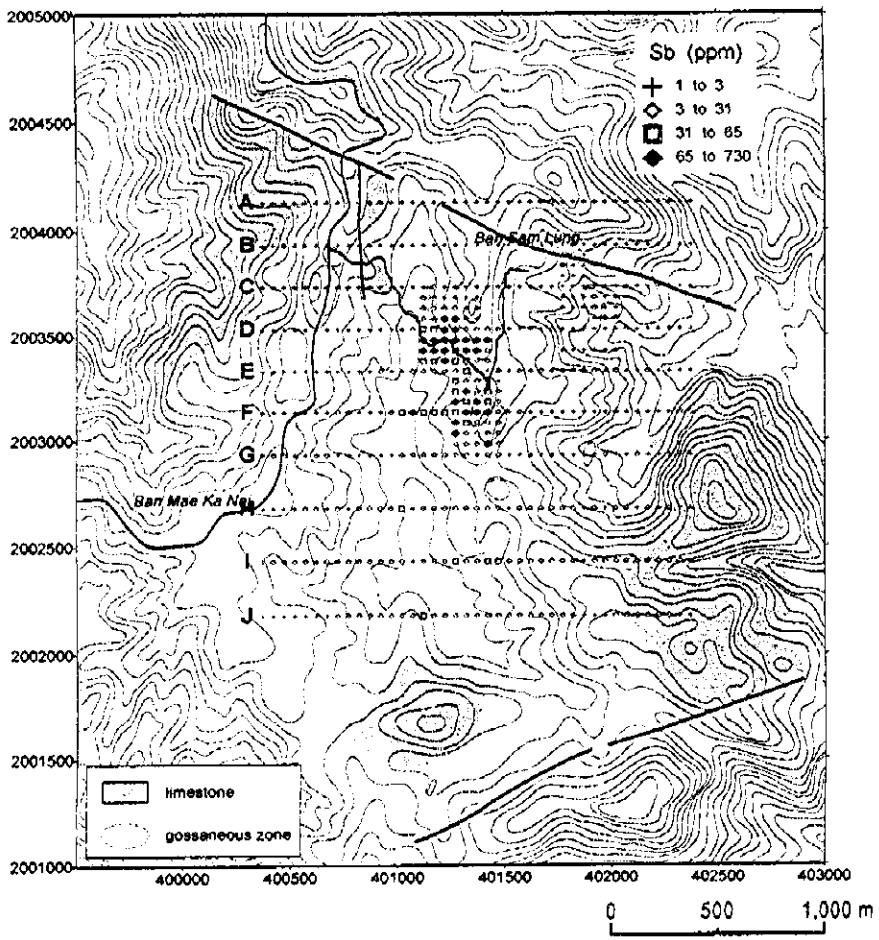

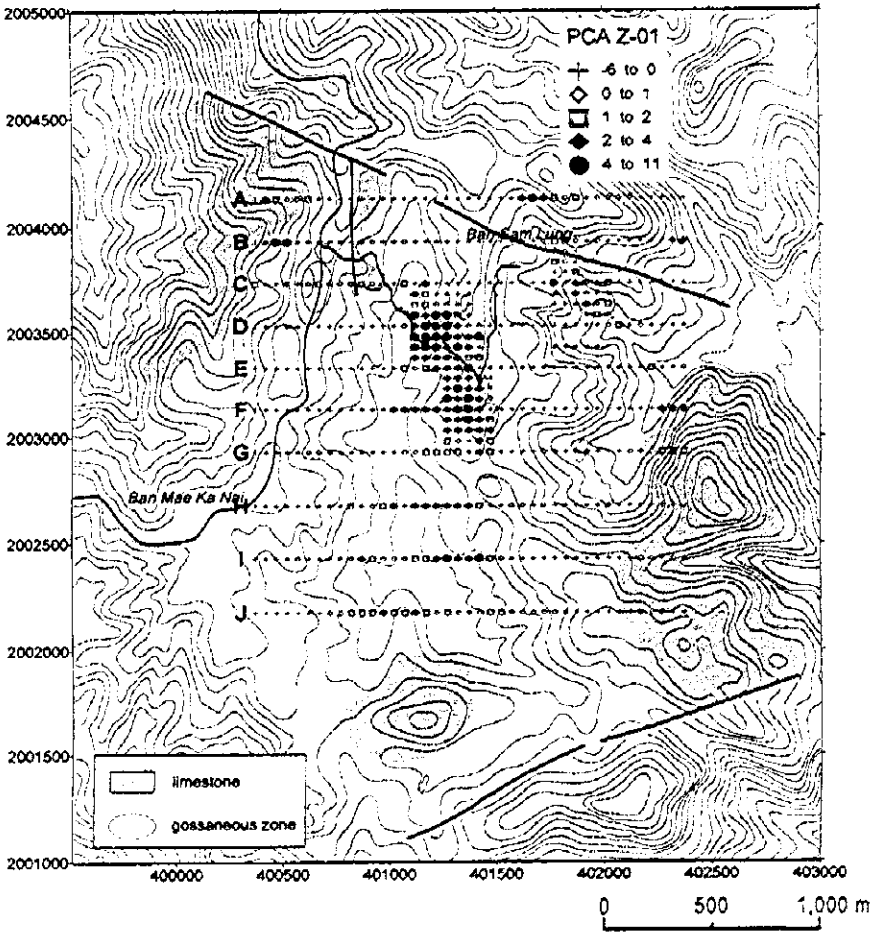

Fig. II-2-5-10 Geochemical map of Sb content and Z-01 score of PCA of the Mae Kanai Area

[Au] The Au anomaly values almost overlap with the Silurian-Devonian sandstone in the northeast of the survey area due to the background of sandstone. Other anomaly values scatter in the survey area.

[Ba] The Ba values of the east side of a line connecting the westernmost of Line A and the easternmost of Line J are higher than those of the west side. There are two Ba anomaly zones. The one anomaly centers on the middle of Line F, the other extends southward from the intersection of Line B on Ban Sam Lung to Line F.

[Fe] The Fe anomaly values are scattered. The samples in the basin have rather high values than those of the east area.

[Hg] The Hg anomaly values center on the middle of Line C and the middle of Line D.

[Mg] The Mg anomaly values also center on the middle of Line C and the middle of Line D. The samples in the limestone area commonly show high Mg content because of the high Mg background of limestone.

[Sb] The anomaly zone of Sb is almost similar to those of Pb.

2-5-2 MMI geochemistry

The Mae Kanai area is widely overlain by unconsolidated sediments and does not provide many outcrops. There is a large possibility that all deposits do not expose on the surface, even if a strata-bounded deposit embeds in the gentle-dipping beds. Therefore the Mobile Metal Ions (MMI) technique is also carried out in the Mae Kanai area, because some mineral indications may be missed by the ordinary soil geochemical technique. It is said that the MMI technique is useful in locating buried mineralization. The pathfinder elements are Zn, Pb, Cu and Cd in consideration of an expected deposit type in this area.

1. Sampling

The MMI soil sample requires the surface soil layer. It is said that the MMI element concentrations are more sensitive to its sampling depth than to its soil horizon. Therefore the samples were collected approximately 50 to 100 mm below the surface at a consistent depth taking no thought of soil horizon by using of plastic garden spades and plastic kitchen colanders, and put into plastic snap seal bags. Then the samples were dispatched to the laboratory.

2. Data processing

The MMI technique is a partial extraction technique of ions that have moved in the weathering zone and are only weakly or loosely attached to surface soil particles. Therefore the MMI analysis values are not the absolute values of elements in the samples. It means that the relative difference between background samples and anomalous samples is important.

For this purpose, the Response Ratio, that is an index of relative difference, was proposed in the manual of the MMI Technology. This is a simple index: the average of the data set that consists of the data less than the lowest qurartile is calculated as a background value; then each analysis value is standarized by dividing the background value.

According to this method, the data set of the Response Ratio of each element is made for the further interpretation.

3. Distribution of geochemical anomaly values

Generally the data of the MMI technique has a large contrast, therefore a sample with a response ratio of 2 or less is a background sample, and a sample with that of 2-5 is a low grade sample. Samples with response ratios greater than 5 are anomalous samples, and they also need to be interpreted weather the anomaly is directly derived from the mineralization.

The response ratios distribution charts of each element are shown in Fig. II-2-5-2 to -5 arranged with the charts of the ordinary soil geochemical survey, in order to compare both results. Samples are classified into 4 levels by response ratios 2, 5 and 10 in the charts.

The distribution of anomaly samples of the MMI method is described as follows. Here a sample with response ratios greater than 5 treats as a low anomaly sample, and that greater than 10 as a high anomaly sample.

[Zn] The MMI Zn anomaly values gather two areas: the area extending from the middle of Line B to the middle of Line G, and the area around Ban Sam Lung. The former almost overlaps with the anomaly of the ordinary soil geochemistry, but the high MMI anomaly values center on the northern part between Line B and Line D. The latter MMI anomaly zone is not detected by the ordinary soil geochemistry.

[Pb] The north-northeast trending Pb MMI anomaly extends from the middle of Line C to the middle of Line F, and another anomaly is widespread in the basin. The former is almost consistent with the anomaly of the ordinary soil geochemistry, but the latter is not detected by the ordinary soil geochemistry. The MMI anomaly values also occur near Ban Sam Lung.

[Cu] The MMI anomaly values of Cu are distributed at the area extending from the middle of Line D to the middle of Line F and at the area around Ban Sam Lung.

[Cd] The distribution of MMI anomaly values of Cd is almost similar to those of Zn. Two MMI anomaly zones are detected: the area extending from the middle of Line B to the middle of Line G, and the area centering on Ban Sam Lung.

2-5-3 Results of the geochemical soil survey

The geochemical anomaly of major three elements, Zn, Pb and Cu are selected and integrated to Fig. II-2-5-11. The chart shows both results of the conventional soil geochemistry and the MMI geochemistry.

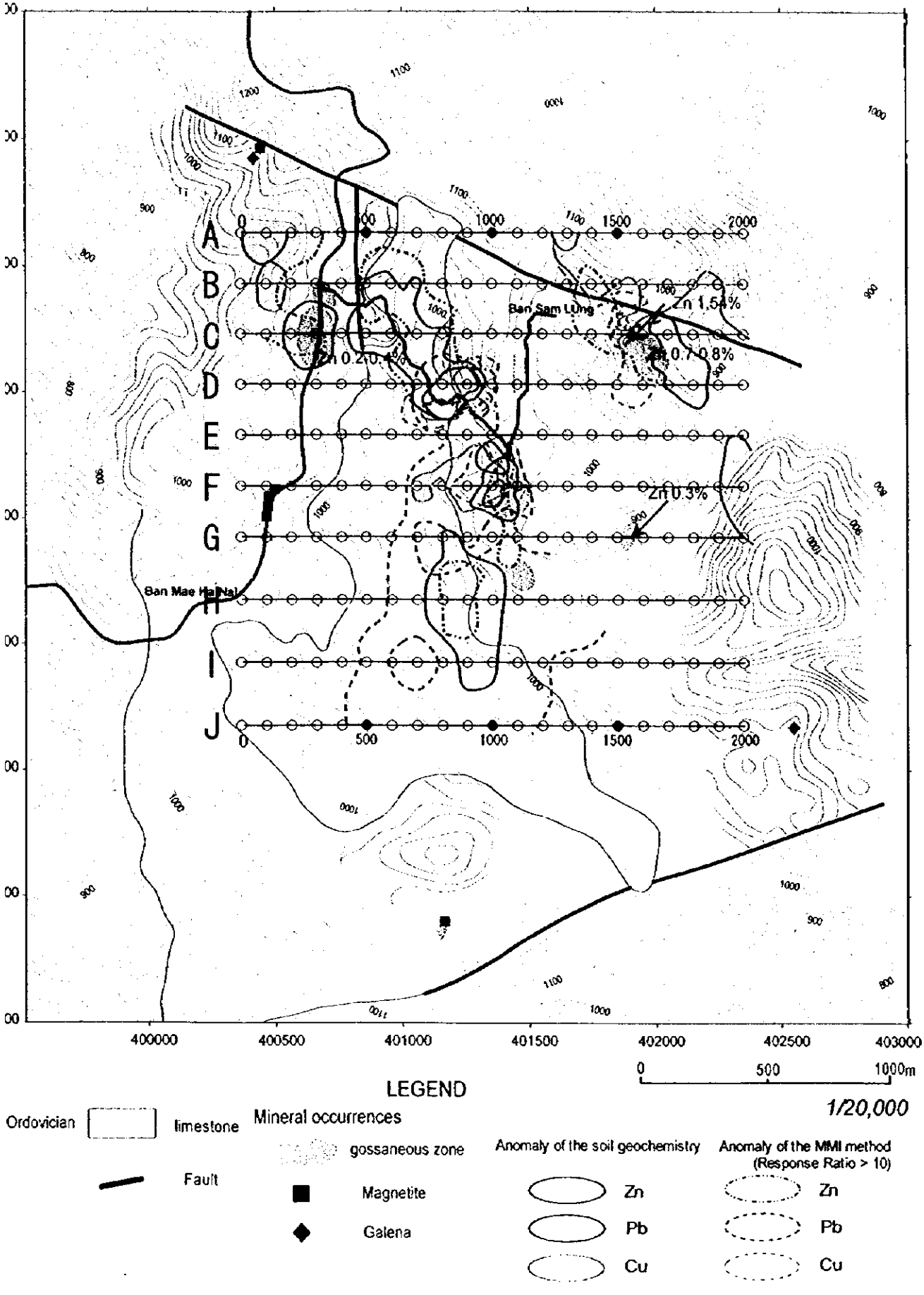

Fig. II-2-5-11 Geochemical interpretation map of the Mae Kanai Area

The Zn anomaly of ordinary geochemistry and those of MMI geochemistry overlap at the following five areas.

a) The gossan zone along the main road centering on the points ranging from C-200 to C-100.

b) The area between the points ranging from B-500 to B-700 and those ranging from D-700 to D-900.

c) The gossan zone centering on the points ranging from F-1000 to F-1200.

d) The gossan zone southeast of Ban Sam Lung crossing with Line C and Line D.

e) The area around the points from H-800 to H-900.

The Pb anomaly zones delineated by two soil geochemical techniques overlap at the following two areas.

a) The area around the points ranging from D-800 to D-900.

b) The area between the periphery of F-1000 and Line E.

The Cu anomaly zones delineated by two soil geochemical techniques overlap at the following two areas.

a) The periphery of D-900.

b) The are between the points ranging from F-800 to F-1000 and Line E.

Therefore two promising areas are confined by the conventional and the MMI geochemical techniques as follows.

1) The area between the gossan zone around F-1000 point and Line E.

2) The periphery of the points ranging from D-800 to D-900.

At the thought of the relation with gossan zones, the gossan zone southeast of Ban Sam Lung is another high potential area. The gossans contain very high zinc contents, though this area is not an overlapping area between the anomaly of the ordinal soil geochemistry and that of the MMI geochemistry. The MMI high anomaly values surround this gossan. It appears that the area is a potential area for a fault-related mineralization, because high anomaly values run parallel with a north striking fault to the north of the gossan zone.

The west side of Line A, Line B and Line C is also potential area for the fault-related mineralization because several gossan zones occur and zinc anomaly values run parallel with a fault.

2-6 Geophysical Survey

2-6-1 Measurement of rock properties

1. Measurement result

The measurement result of rocks and ore samples were shown in Table II-2-6-1, Fig. II-2-6-1. Also, the rock acquisition location of the Mae Kanai area was shown in Fig.II-2-6-2.

In the Mae Kanai area, it acquired 31 samples. The apparent resistivity shows from 3 to 69600

Ω·m value and the chargeability shows a maximum of 134mV·sec/V.

The resistivity shows generally high value, many samples show more than 1000Ω·m. All samples of limestone (12 samples) show high resistivity. Skarn (MMR-03) shows high resistivity and dolomite (MMR-09,MMR-10,MMR-25) show relatively high value. The sample of gossan (MMR-32) and silicified rock (MMR-19) show low resistivity less than 10Ω·m. MMR-32 was acquired from the gossan near station 1500 of Line G. MMR-19 was acquired from the mineral occurrence 800m south of station 800 of Line J.

The chargeability shows generally high value, but the sample of shale(MJ-11,MJ-12,MMR-29) and granite(MMR-07) show low value. 7 samples shows high chargeability more than 30mV·sec/V. Limestone(MMR-12,MMR-13) were acquired near station 2000 of Line I, and it shows about 40mV·sec/V. The samples of gossan (MJ-08,MMR-31,MMR-32) show high value more than 50mV·sec/V. MJ-08 was acquired from the gossan near station 1000 of Line F. MMR-31 and MMR-32 were acquired from the gossan near station 1500 of Line G. MMR-32 shows highest value (134mV·sec/V), and the resistivity shows less than 10Ω·m. Also, calc-silicate rock (MMR-02) was acquired from the stream 400m north of station 100, and it shows 82mV·sec/V. Silicified rock (MMR-19) shows high value (97mV·sec/V) and the resistivity shows less than 10Ω·m.

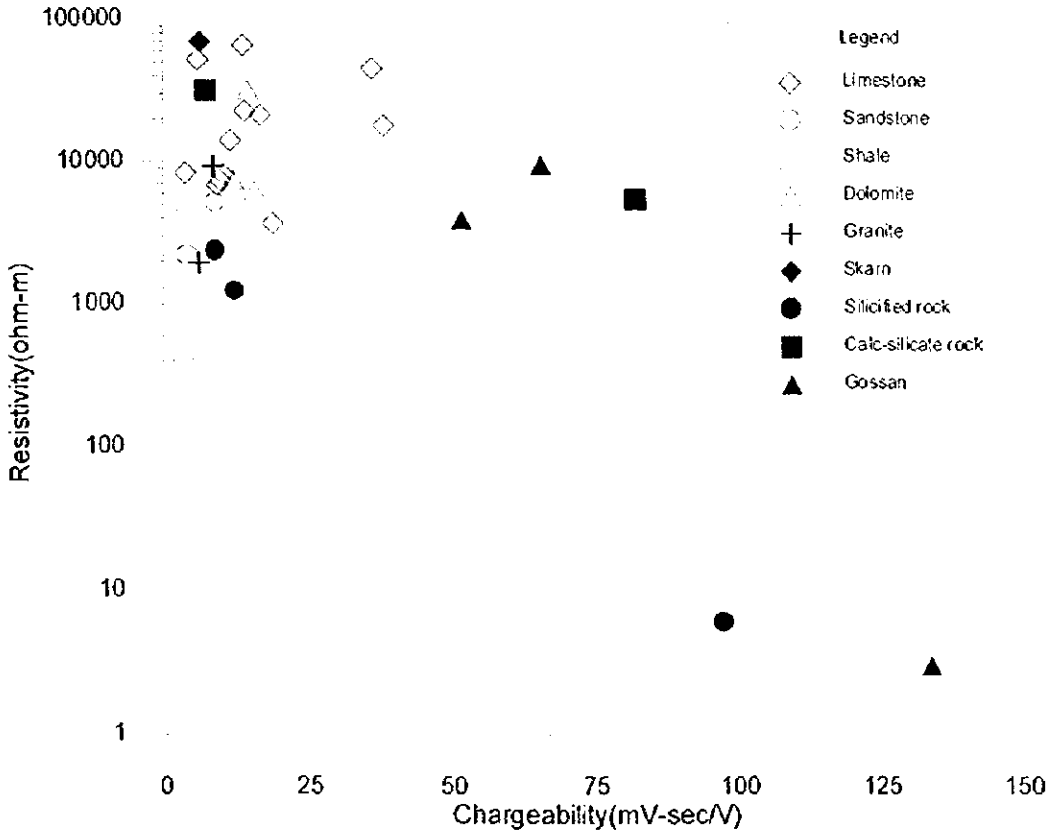

Fig.II-2-6-1 Resistivity and chargeability of rock sample in the Mae Kanai area

TableII-2-6-1 Resistivity and chargeability of rock samples in the Mae Kanai area

Sample name	Rock name	Resis. (Ω·m)	Charge. (mV · sec/V)
MJ-03	Brecciated silicified rock	1228	12.2
MJ-04	Argillaceous dolomitic limestone	8123	10.3
MJ-05	Siliceous limestone	65500	13.8
MJ-08	Gossan	9518	65.8
MJ-10	Banded limestone	52200	6.0
MJ-11	Black shale	5396	3.1
MJ-12	Silicified shale	476	3.2
MJ-13	Brecciated silicified rock	2360	8.9
MKR-01	Argillaceous limestone	3663	18.9
MKR-09	Dolomitic limestone	22600	14.0
MMR-01	Quartz rich sandstone	5116	9.0
MMR-02	Calc-silicate rock with magnetite dissemination	5169	82.4
MMR-03	Pyroxene-garnet skarn	69600	6.4
MMR-04	Calc-silicate rock	31600	7.3
MMR-07	K-feldspar porphyritic biotite granite	1941	6.0
MMR-09	Dolomite	7363	12.0
MMR-10	Dolomite	6231	15.7
MMR-11	Argillaceous limestone	8350	3.8
MMR-12	Argillaceous limestone	18000	38.3
MMR-13	Argillaceous limestone	45200	36.4
MMR-15	Midium grained sandstone	2210	4.2
MMR-19	Brecciated silicified rock with manganese oxide	6	97.4
MMR-24	Argillaceous limestone	7374	9.8
MMR-25	Dolomite	31670	14.6
MMR-29	Black shale	346	3.6
MMR-31	Gossan	3898	52.0
MMR-32	Gossan	3	134.0
MQ-01	Fine grained biotite granite	9278	8.5
MQ-07	Argillaceous limestone	6792	9.3
NR-18	Bedded limestone	21200	16.7
NR-20	Limestone	14000	11.5

2-6-2 Mae Kanai area

1. Line setting

In this area, it set total line length of 20 km in amount which 10 × 2.0 km length with the direction of E-W.

The line locations are shown in Fig.II-2-6-3.

2. Measurement result

(1) Line A (Fig.II-2-6-4)

The apparent resistivity shows from 40Ω·m to 4965 Ω·m value. The apparent resistivity shows more than roughly 300 Ω·m at the east of station 1500, and especially the apparent

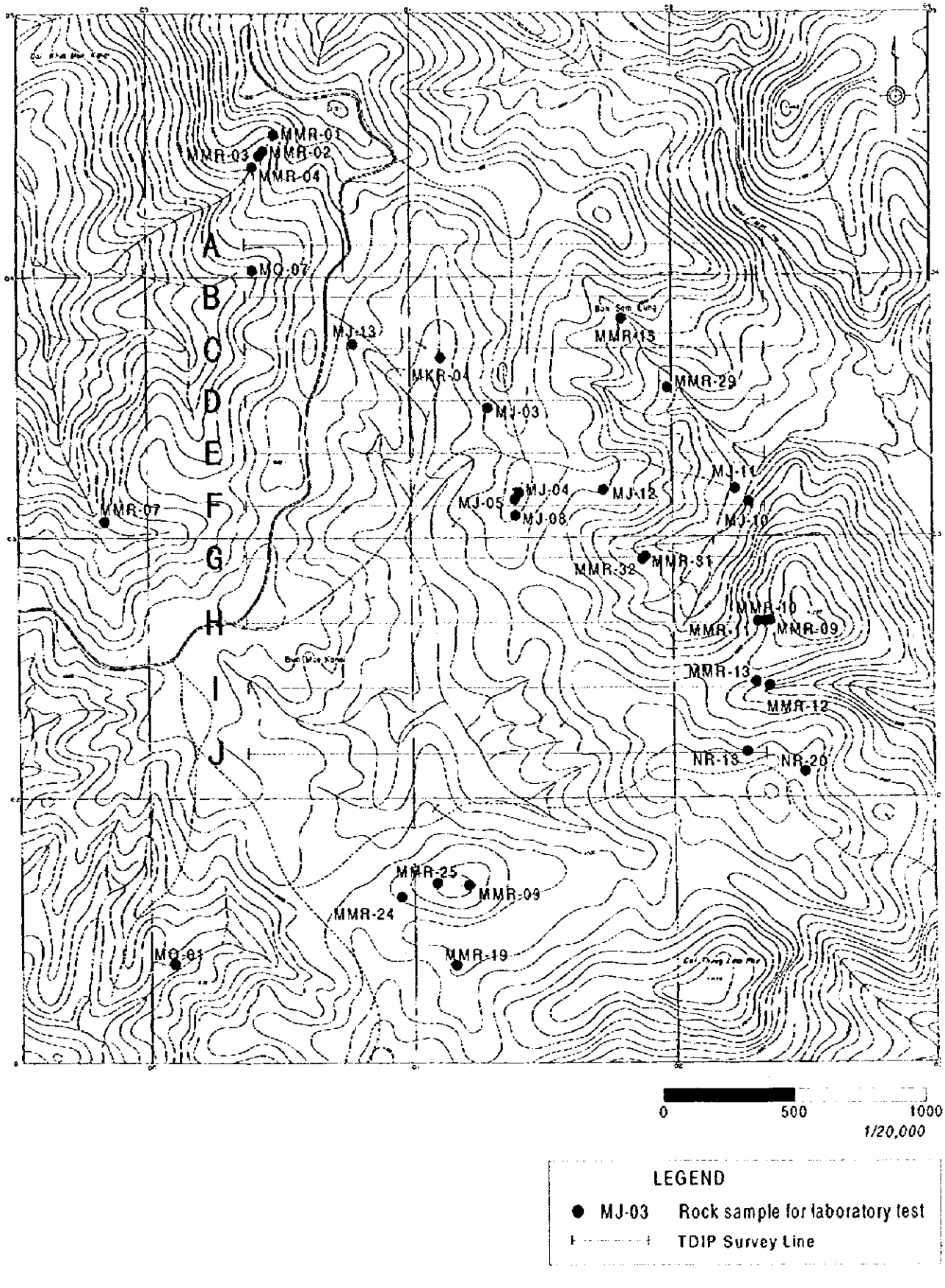

Fig.II-2-6-2 Locality of rock sample for laboratory test in the Mae Kanai area

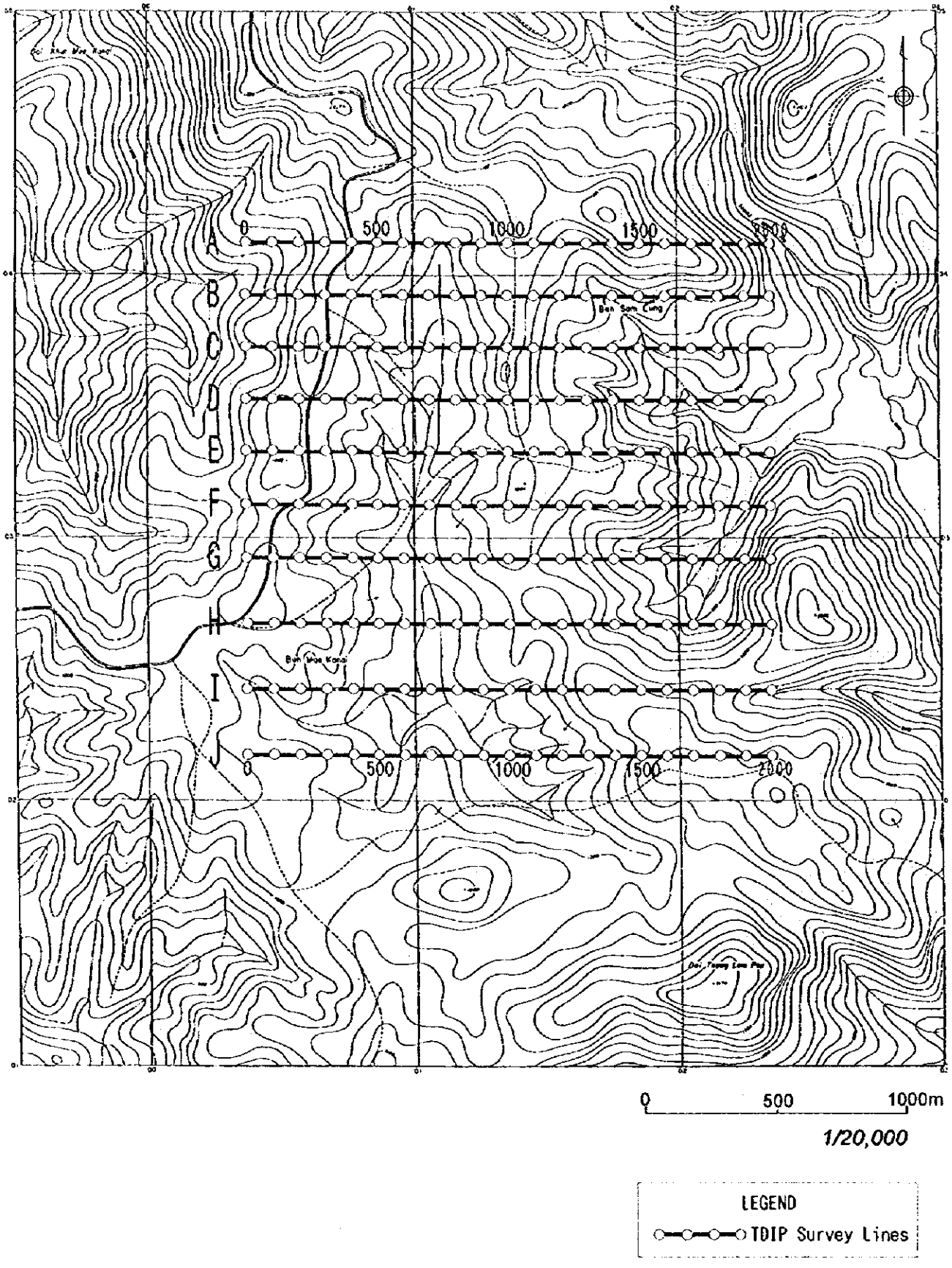

Fig.II-2-6-3 Location of survey line in the Mae Kanai area

resistivity shows high value of 4965Ω·m (N=1) in the shallow part of station 1800. The apparent resistivity shows approximately less than 300 Ω·m at the west of station 1500. Also, the part witch shows the apparent resistivity of less than 60 Ω·m is seen in the shallow part between station 400 and 1000. And the resistivity shows low value in the shallow part between station 200 and 300, in the middle part of station 1400.

The chargeability shows more than 15mV·sec/V from the shallow part of station 400 to the deep part of station 300, from the shallow part of station 800 to the deep part of station 900.

(2) Line B (Fig.II-2-6-5)

The apparent resistivity shows from 35Ω·m to 4367Ω·m value. The apparent resistivity shows high value at the east of station 1500 in the shallow part. This distribution is similar to that of Line A. Especially, the apparent resistivity shows high value of 4367Ω·m (N=1) in the shallow part of station 1800. The apparent resistively of less than 200Ω·m distributes at the west of station 1400. The part which shows low apparent resistivity of less than 50Ω·m is seen from the shallow part of station 800 to the deep part of station 900. Also, the apparent resistivity shows low value in the shallow part of station 500.

The chargeability of this line shows highest value in all survey lines and shows more than 30mV·sec/V from the shallow part of station 400 to the deep part of station 700. Especially, the chargeability shows high value of 53mV·sec/V in the deep part (N=1) of station 700.

(3) Line C (Fig.II-2-6-6)

The apparent resistivity shows from 56Ω·m to 1903Ω·m value. The high apparent resistivity of more than 1000Ω·m is seen in the shallow part of station 1000. Also, the high apparent resistivity is seen in the shallow part between station 200 and 300. The low apparent resistivity of less than 100Ω·m is seen between station 500 and 800 in the deep part.

As for the chargeability, the center of high chargeability is seen between station 300 and 400 in the deep part, and the high chargeability of more than 20mV·sec/V is seen between station 200 and 700 in the middle and the deep part. Also, the chargeability shows relatively high value in the deep part of station 1600.

(4) Line D (Fig.II-2-6-7)

The apparent resistivity shows from 136Ω·m to 2688Ω·m value. The high apparent resistivity of more than 1000Ω·m is seen at the west of station 200, at the east of station 1900 and in the shallow part of station 1200. The apparent resistivity is generally high, but it shows less than 200Ω·m between station 500 and 700 in the deep part.

The chargeability is generally low, but it shows about 20mV·sec/V from the deep part of station 1700 to the middle part of station 1800.

(5) Line E (Fig.II-2-6-8)

The apparent resistivity shows from 124Ω·m to 3881Ω·m. The apparent resistivity shows high value at the west of station 200, between station 1400 and 1700. The apparent resistivity shows less than 400Ω·m between station 300 and 900.

The chargeability shows high value at the west end and the east end of this line. Especially, the chargeability shows more than 20mV·sec/V at the east of station 1700.

(6) Line F (Fig.II-2-6-9)

The apparent resistivity shows from 52Ω·m to 5486Ω·m value. Generally, the distribution of the apparent resistivity is similar to that of line E. The high apparent resistivity distributes at the east part of this line, and center of high value is seen in the shallow part of station 1600. The low apparent resistivity of less than 150Ω·m is seen from the shallow part of station 500 to the deep part of station 700. Also, the apparent resistivity shows relatively low value from the shallow part of station 500 to the deep part of station 300, and this distribution shows the convex type.

The chargeability distribution is similar to that of line E, too, and the chargeability shows relatively high value at the west end and the east end of this line. The chargeability shows about 20mV·sec/V in the middle part of station 1600.

(7) Line G (Fig.II-2-6-10)

The apparent resistivity shows from 94Ω·m to 1473Ω·m value. Generally, the apparent resistivity shows more than 300Ω·m at the east of station 1000, and it shows less than 300Ω·m at the west of station 1000. The apparent resistivity does not show very low value, but it is relatively low in the deep part of station 800.

The chargeability shows generally low value. The chargeability of more than 20mV·sec/V is not seen, and the chargeability shows 15mV·sec/V at the west end of this line.

(8) Line H (Fig.II-2-6-11)

The apparent resistivity shows from 109Ω·m to 2331Ω·m value. The distribution of apparent resistivity is similar to that of line G, it shows more than 300Ω·m at the east of station 1000, and it shows less than 300Ω·m at the west of station 1000. The low apparent resistivity of less than 150Ω·m is seen from the shallow part of station 600 to the deep part of station 800. Also, the low apparent resistivity is seen from the middle to the deep part of station 300.

The chargeability shows relatively low value, and the chargeability of more than 15mV·sec/V is not seen.

(9) Line I (Fig.II-2-6-12)

The apparent resistivity shows from 127Ω·m to 1558Ω·m value. The distribution of apparent

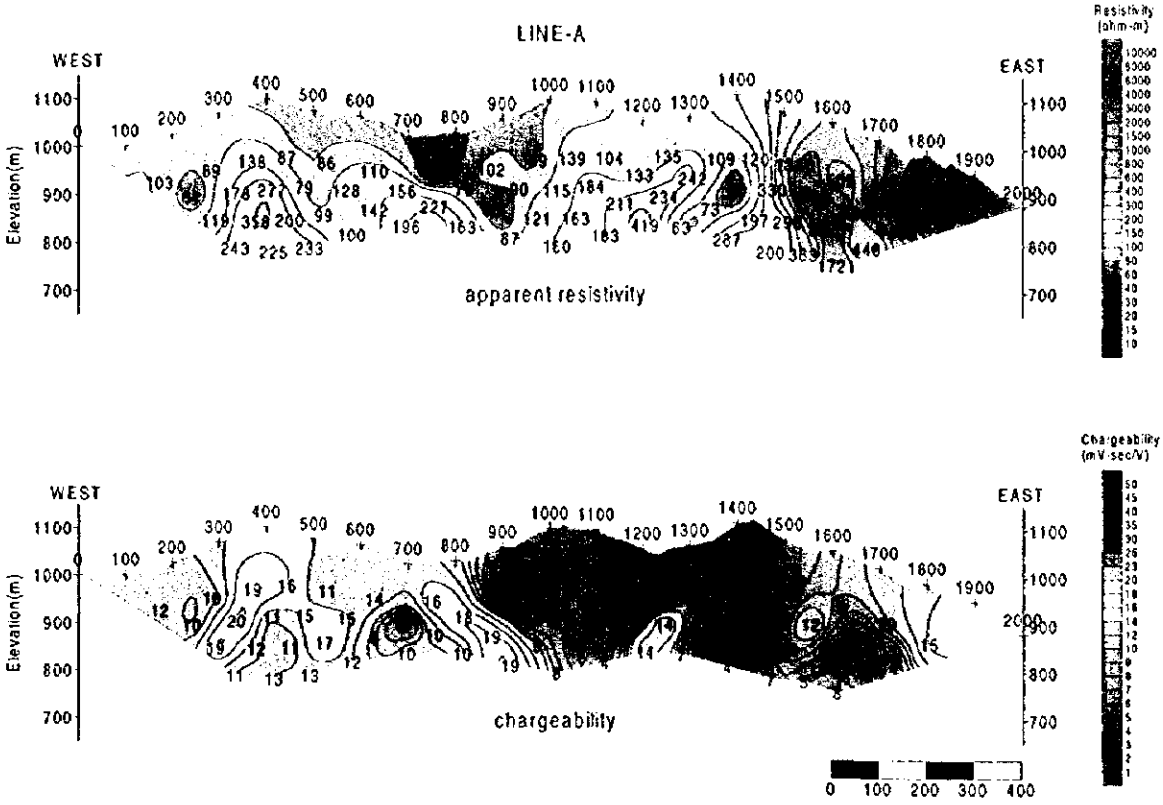

Fig.II-2-6-4 Pseudosection of apparent resistivity and chargeability of the Mae Kanai area(A)

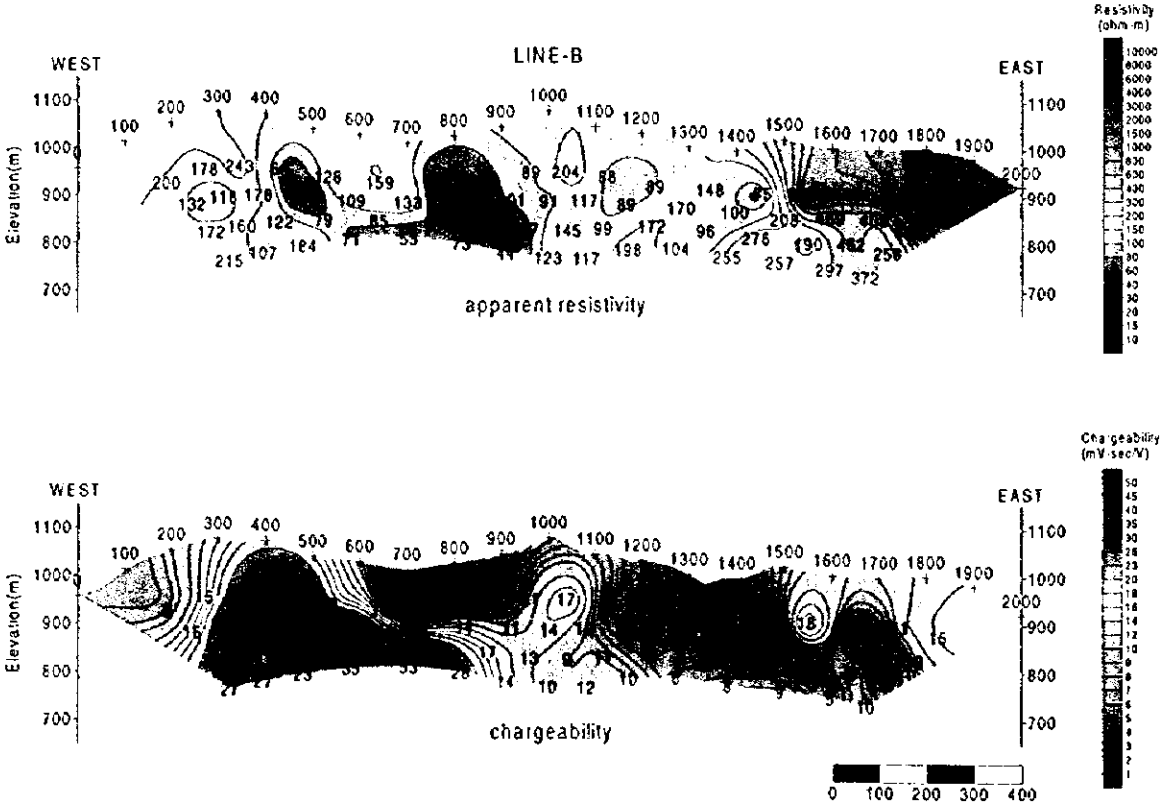

Fig.II-2-6-5 Pseudosection of apparent resistivity and chargeability of the Mae Kanai area(B)

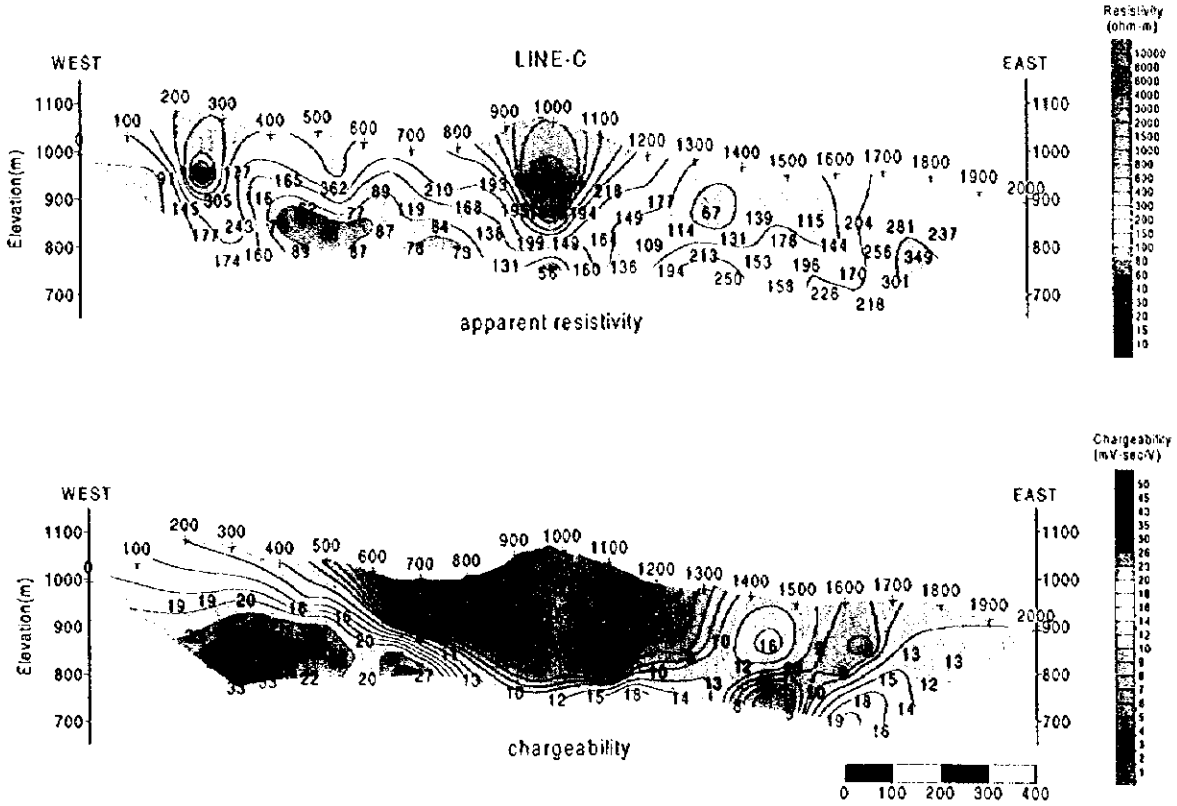

Fig.II-2-6-6 Pseudosection of apparent resistivity and chargeability of the Mae Kanai area(C)

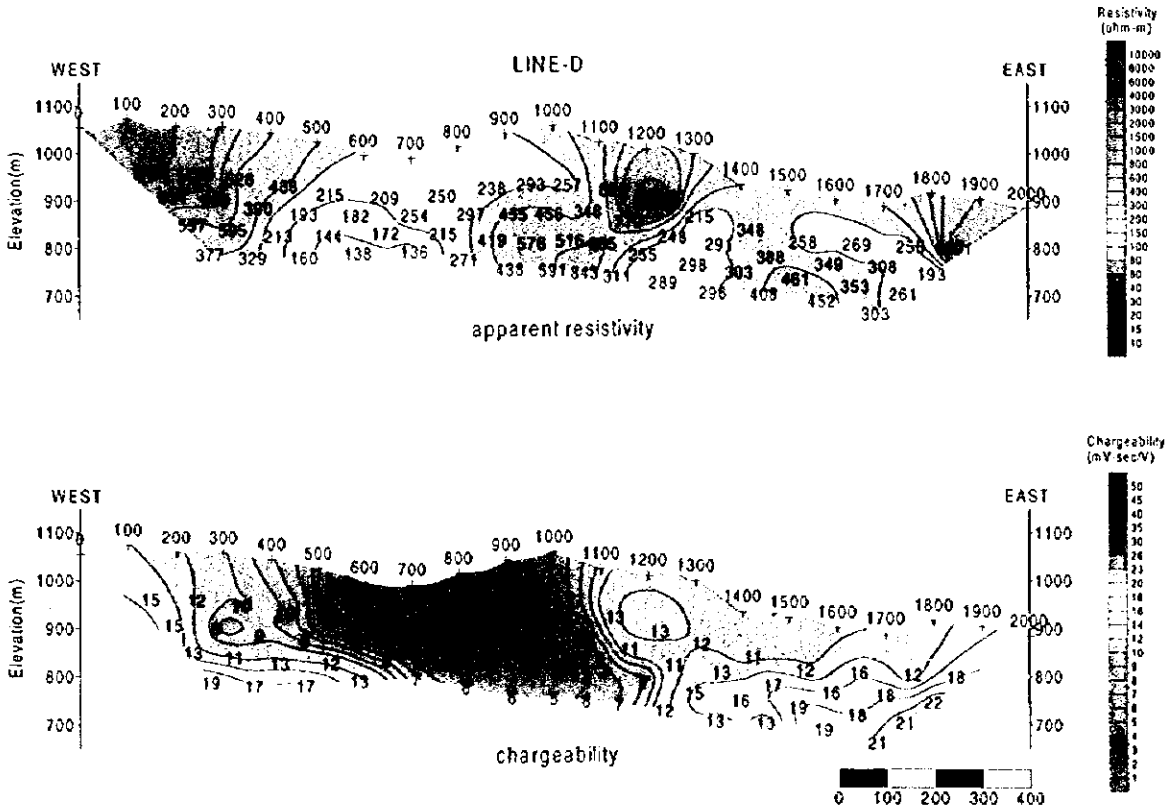

Fig.II-2-6-7 Pseudosection of apparent resistivity and chargeability of the Mae Kanai area(D)

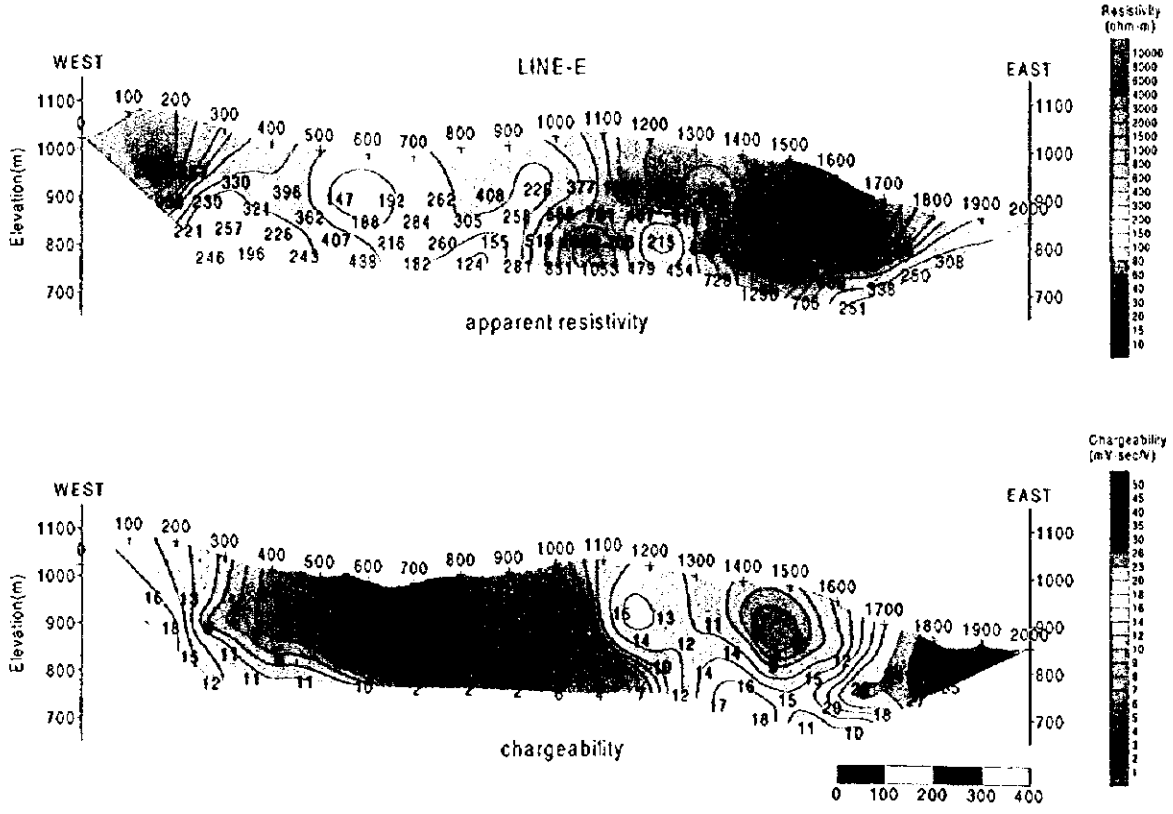

Fig.II-2-6-8 Pseudosection of apparent resistivity and chargeability of the Mae Kanai area(E)

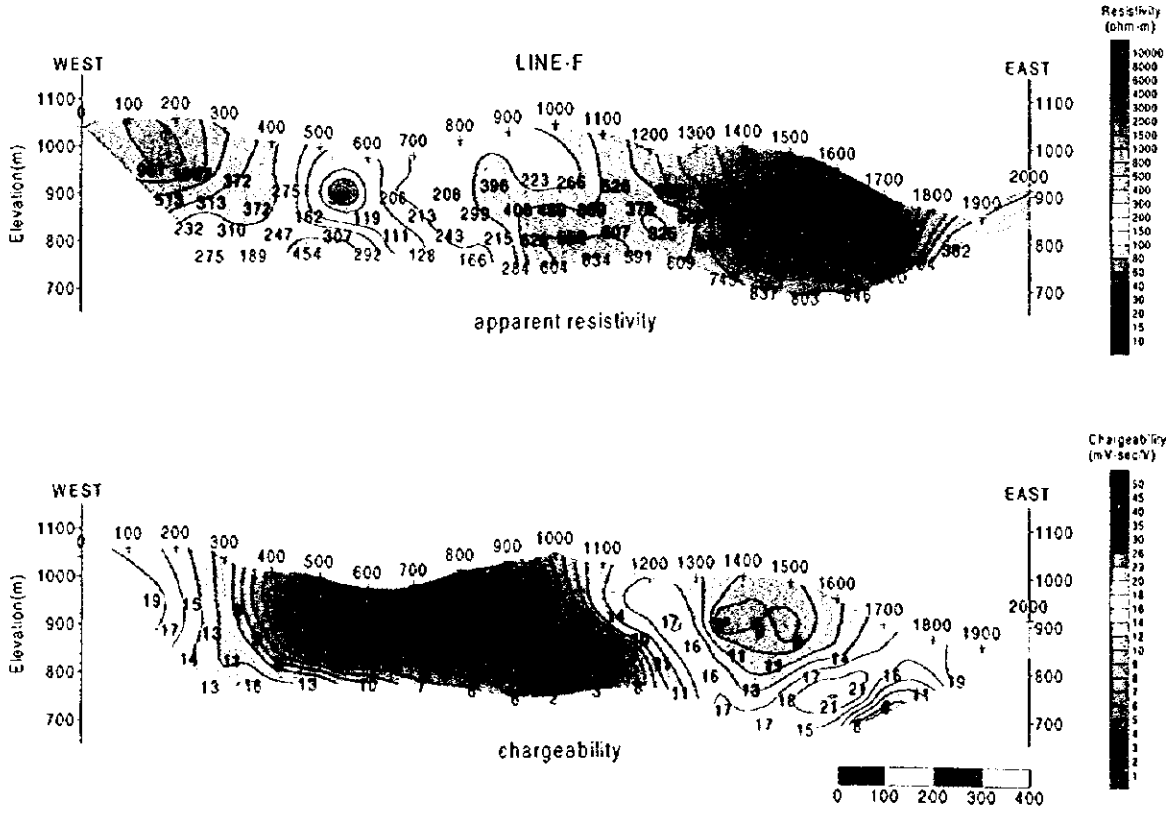

Fig.II-2-6-9 Pseudosection of apparent resistivity and chargeability of the Mae Kanai area(F)

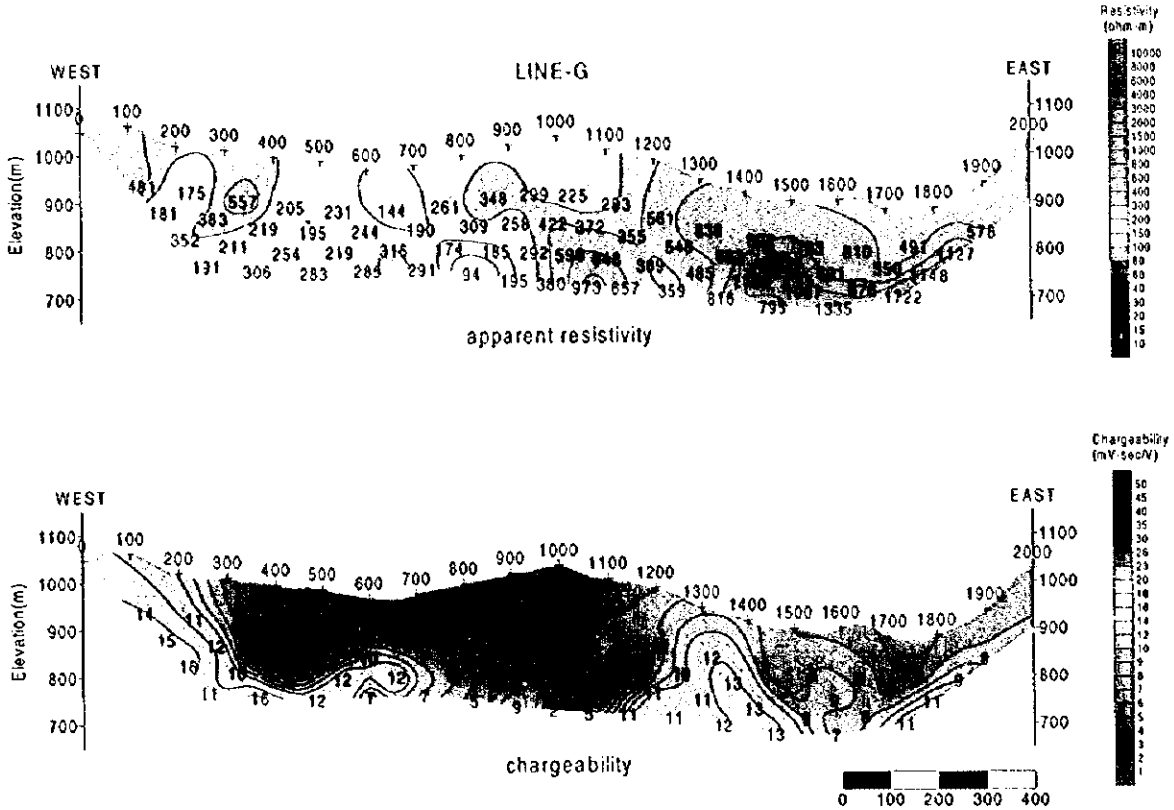

Fig.II-2-6-10 Pseudosection of apparent resistivity and chargeability of the Mae Kanai area(G)

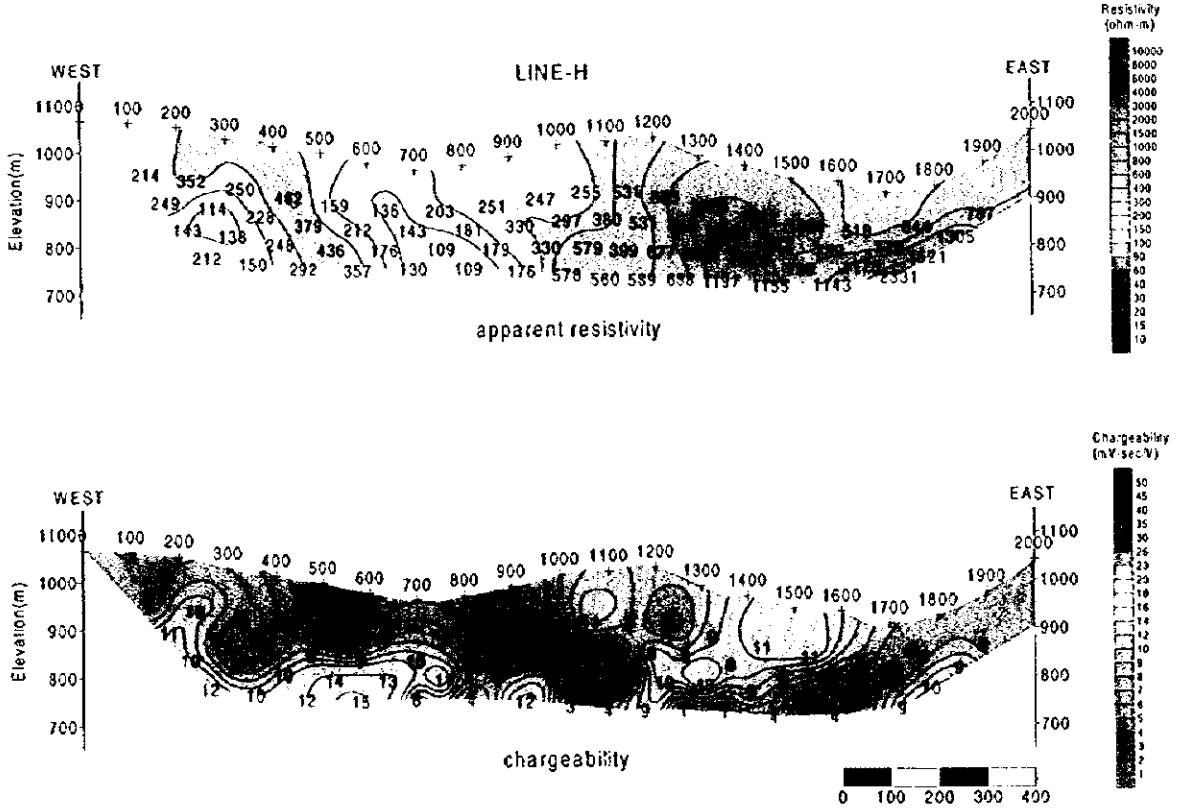

Fig.II-2-6-11 Pseudosection of apparent resistivity and chargeability of the Mae Kanai area(H)

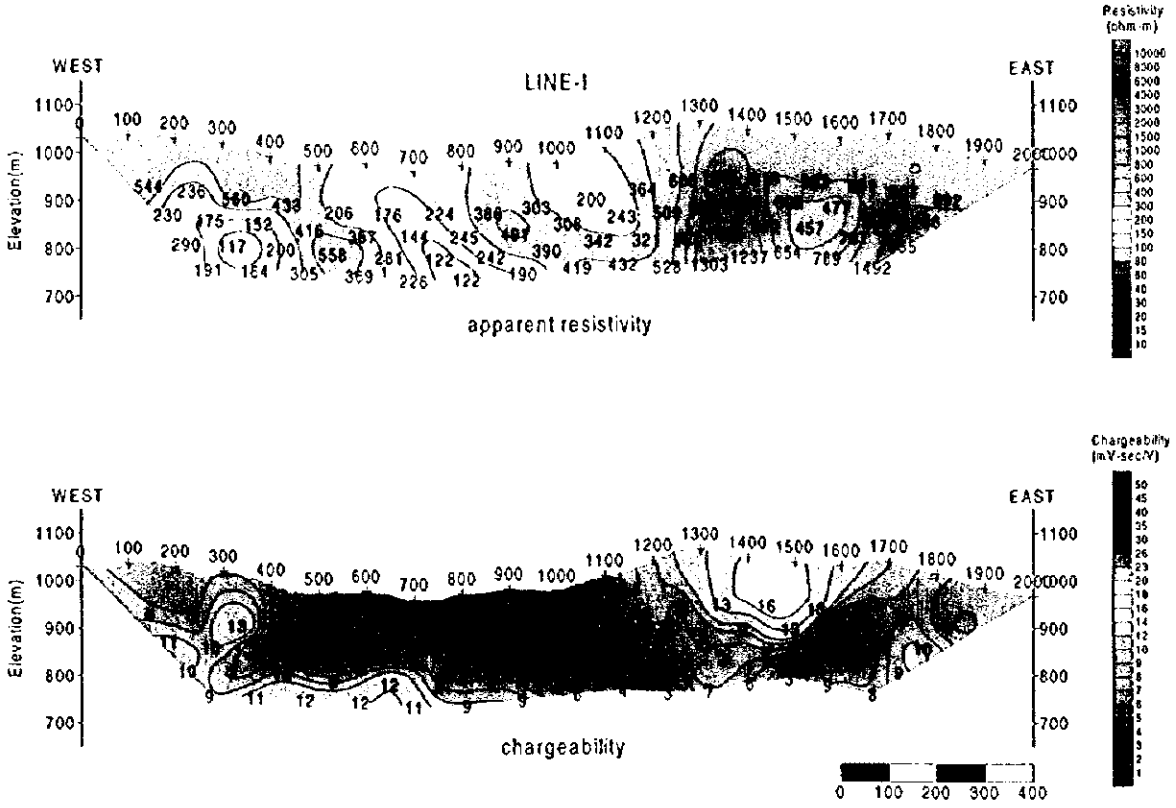

Fig.II-2-6-12 Pseudosection of apparent resistivity and chargeability of the Mae Kanai area(I)

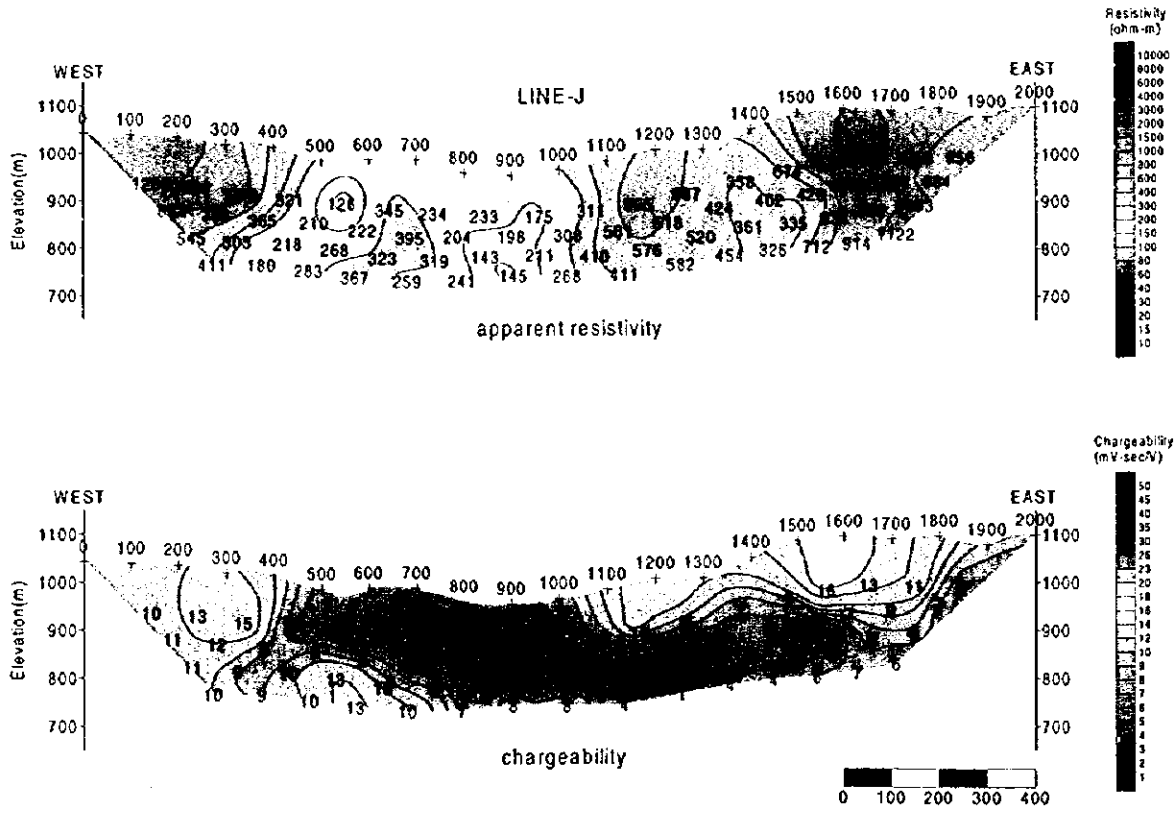

Fig.II-2-6-13 Pseudosection of apparent resistivity and chargeability of the Mae Kanai area(J)

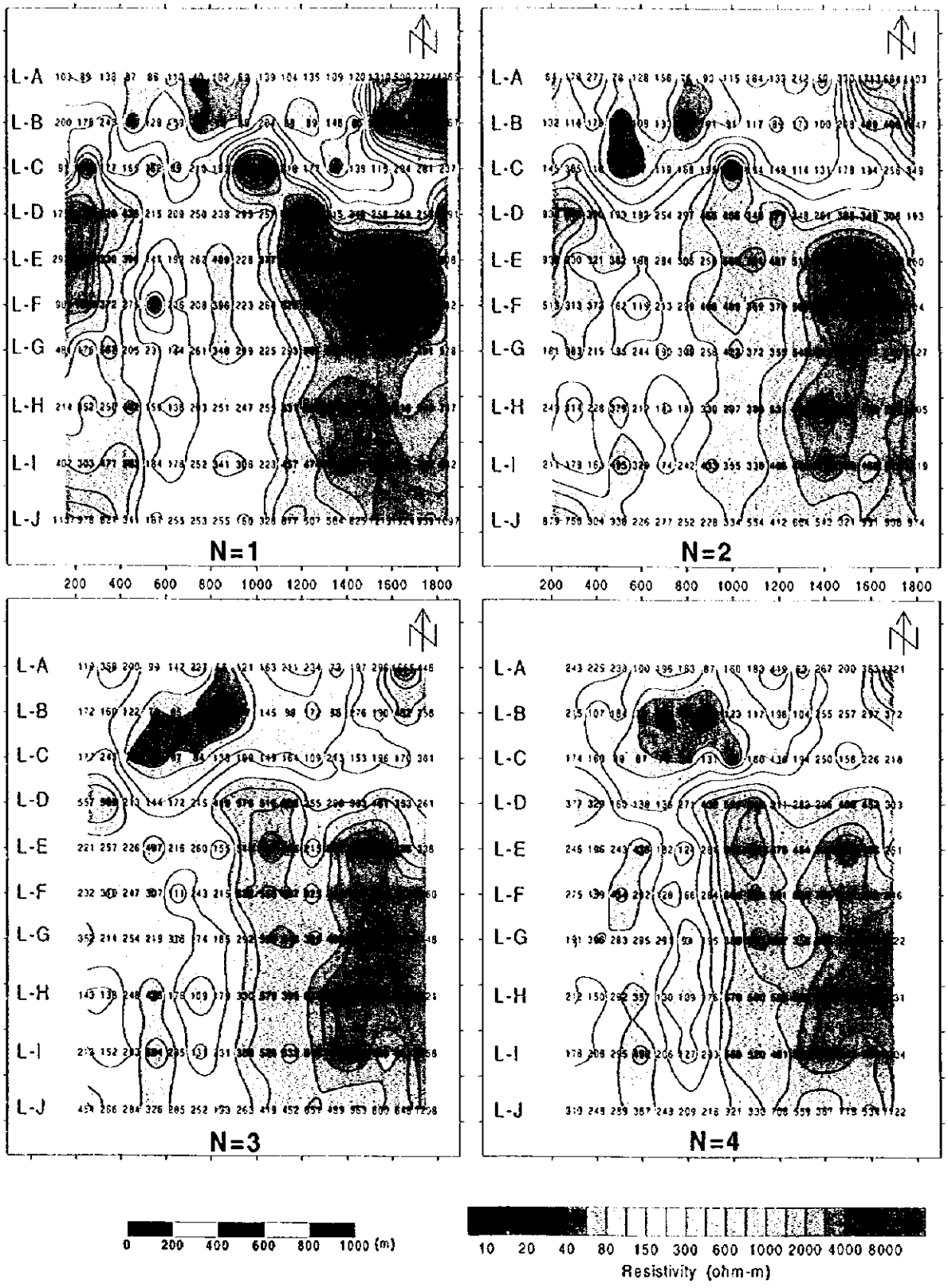

Fig.II-2-6-14 Plan map of apparent resistivity of the Mae Kanai area

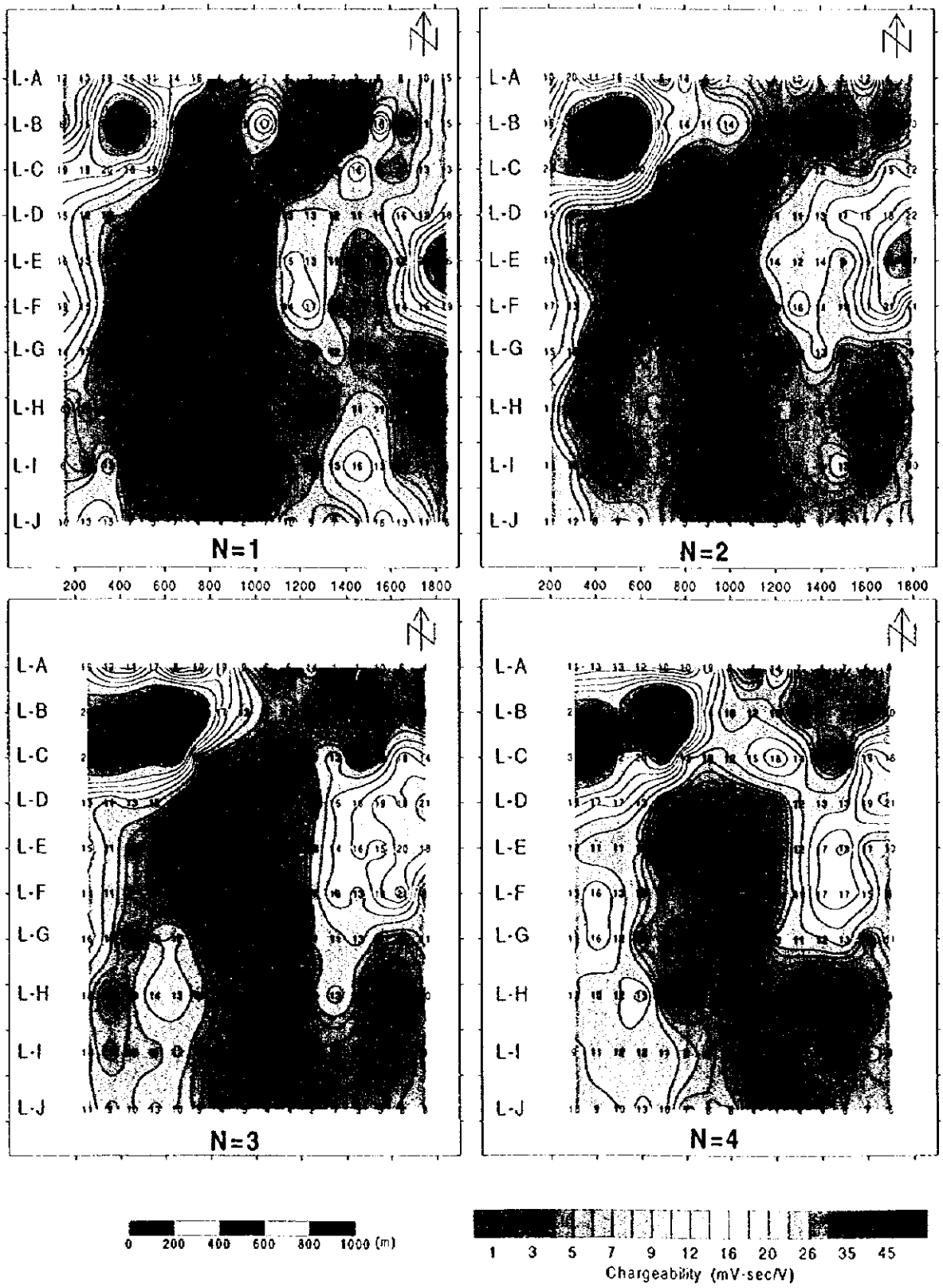

Fig.II-2-6-15 Plan map of chargeability of the Mae Kanai area

resistivity is similar to that of line H, it shows more than 300Ω·m at the east of station 1000. The low apparent resistivity of less than 200Ω·m is seen from the shallow part of station 600 to the deep part of station 800. Also, the low apparent resistivity is seen from the middle to the deep part of station 300.

The chargeability shows relatively low value, and it shows only 16mV·sec/V in the shallow part of station 1500.

(10) Line J (Fig.II-2-6-13)

The apparent resistivity shows from 180Ω·m to 1924Ω·m value. The apparent resistivity shows generally high value, but the apparent resistivity from 200 to 300Ω·m is widely distributed between station 500 and 1000.

The chargeability shows relatively low value, and it shows only 16mV·sec/V in the shallow part of station 1500.

(11) Apparent resistivity plan map (Fig.II-2-6-14)

When seeing the result of N=1, the apparent resistivity of less than 200 Ω·m distributes from Line A to Line C at the north part of this area. It is narrowing the distribution range of the low apparent resistivity part as the depth increases (N becomes big). In the shallow part, the center of the low apparent resistivity is seen at Line A. But in the deep part, it is seen at Line B. Also, the low apparent resistivity of less than 200 Ω·m distributes from Line E to Line I as the narrow shape of N-S direction, and the apparent resistivity shows more than 300Ω·m at the both side of this low apparent resistivity zone. It is narrowing the distribution range of the low apparent resistivity part as the depth increases, but it is also wide in the deep part (N=4). This low apparent resistivity zone of N-S direction is shifted to the east as the depth increases.

(12) Chargeability plan map (Fig.II-2-6-15)

When seeing the result of N=1, the chargeability of more than 20mV·sec/V is spreading from Line A to line C, and the center of the high chargeability part is located at the station 400 of Line B. It is spreading the distribution range of the high chargeability part as the depth increases, and the center of the high chargeability part is shifted to the east (station 700) in the deep part (N=4). Also, the high chargeability part of more than 20mV·sec/V is seen at the east end of Line E, but it is narrowing the distribution range as the depth increases. Except these two parts, the high chargeability part is not seen.

3. Analysis result of 2-D

(1) Line A (Fig.II-2-6-16)

The resistivity shows more than 400Ω·m at the east of station 1600, and the resistivity is higher to the east. The resistivity shows low value at the west of station 1500 in the shallow part,

and the center of the low resistivity is seen in the shallow part of station 700. The resistivity discontinuity is estimated between station 1500 and 1600, because the resistivity value changes sharply around here.

The chargeability shows 15mV·sec/V in the shallow part of station 400 and 700, but high chargeability value is not seen.

(2) Line B (Fig.II-2-6-17)

The resistivity shows high value at the east of station 1600 like that of Line A. The resistivity shows relatively low value at the west of station 1500 compared with that of Line A. The low resitivity of less than 100Ω·m distributes between station 600 and 900, the center of the low resistivity is seen around 800m above sea level under station 800.

The chargeability of this line shows the highest value in this area, and the chargeability shows high value at the west of station 1000. The center of the high chargeability is seen around 800m above sea level under station 500, the chargeability shows high value more than 30mV·sec/V between station 300 and 800 in the deep part. This high chargeability part is spread to the shallow part of station 400.

(3) Line C (Fig.II-2-6-18)

The tendency of the resistivity distribution is relatively similar to that of Line B. The center of the low resitivity is seen around 750m above sea level under station 700, the low resistivity of less than 100Ω·m is widely distributed between station 500 and 1000 in the middle and the deep part.

The chargeability shows high value at the west end of this line, it shows high value around 800m above sea level between station 100 and 400 in the deep part. This chargeability shows lower value as the depth decreases, but the part of more than 30mV·sec/V is widely spread between station 0 and 600 in the deep part. The high chargeability part is shifting to the west compared with that of Line B.

(4) Line D (Fig.II-2-6-19)

The resistivity value is generally high compared with that of Line C, the low resistivity part is seen only between station 500 and 600 in the deep part.

The chargeability distribution is similar to that of Line C, the west side in the deep part shows lower value. The chargeability does not show high value like that of Line C, but the part of more than 20mV·sec/V is seen between station 0 and 500 in the deep part. Also, for the east side, the part of more than 20mV·sec/V is seen between station 1700 and 2000 in the deep part.

(5) Line E (Fig.II-2-6-20)

The resistivity shows more than roughly 400Ω·m at the east of station 800. The high resistivity

part distributes between station 1200 and 1800 in the shallow part. The low resistivity part of less than 100Ω·m is not seen, but the resistivity shows relatively low value less than 200Ω·m between station 0 and 600 in the deep part.

The chargeability distribution is similar to that of Line D, the chargeability shows more than 20mV·sec/V in the deep part of the west end and in the shallow part of the east end.

(6) Line F (Fig.II-2-6-21)

The resistivity shows generally high value, the resistivity of less than 200Ω·m distributes between station 500 and 600. The resistivity shows relatively high value at the both side of this low resistivity zone. Also, the high resistivity of more than 1000Ω·m distributes between the station 1300 and 1700 in the shallow part.

The chargeability distribution is similar to that of Line E, the chargeability shows relatively high value in the deep part of the west end and in the shallow part of the east end, but the part of more than 20mV·sec/V is not seen.

(7) Line G (Fig.II-2-6-22)

The resistivity shows generally high value, but the resistivity of less than 200Ω·m is seen in the shallow part of station 600.

The chargeability is generally low. It shows relatively high value in the deep part of the west end, but the part of more than 20mV·sec/V is not seen.

(8) Line H (Fig.II-2-6-23)

The resistivity distribution is similar to that of Line G. The resistivity shows more than 300Ω·m at the east of station 1000, and shows roughly from 150 to 300Ω·m at the west of station 1000. The resistivity discontinuity is estimated around station 1000, because the resistivity value changes sharply around here.

The chargeability is generally low. It shows relatively high value in the deep part of station 600, but the part of more than 20mV·sec/V is not seen.

(9) Line I (Fig.II-2-6-24)

The resistivity shows more than 300Ω·m at the east of station 1000 like that of Line H. The resistivity from 200 to 300Ω·m distributes widely at the west of station 1000.

The chargeability distribution is roughly similar to that of Line H, and the part of more than 20mV·sec/V is not seen.

(10) Line J (Fig.II-2-6-25)

The resistivity from 200 to 600Ω·m is widely distributed, and the anomaly part is not seen.

The chargeability is generally low, and the anomaly part is not seen.

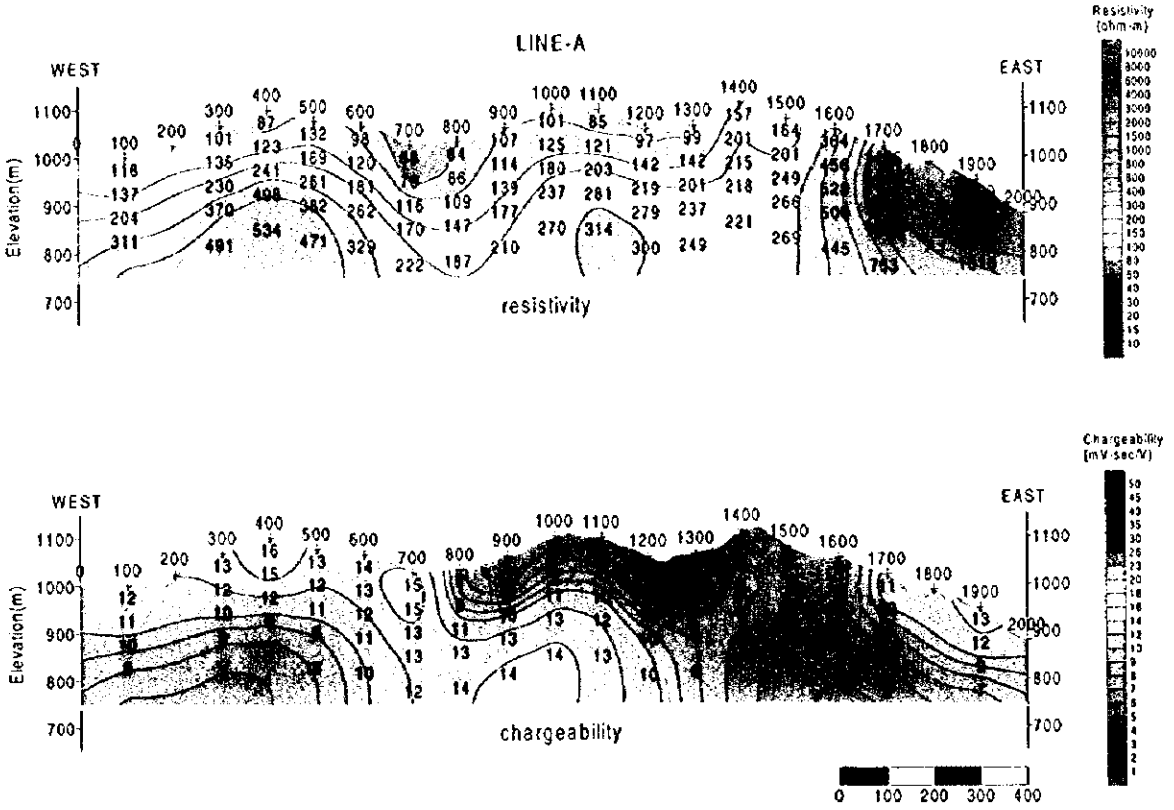

Fig.II-2-6-16 Results of model simulation of the Mae Kanai area(A)

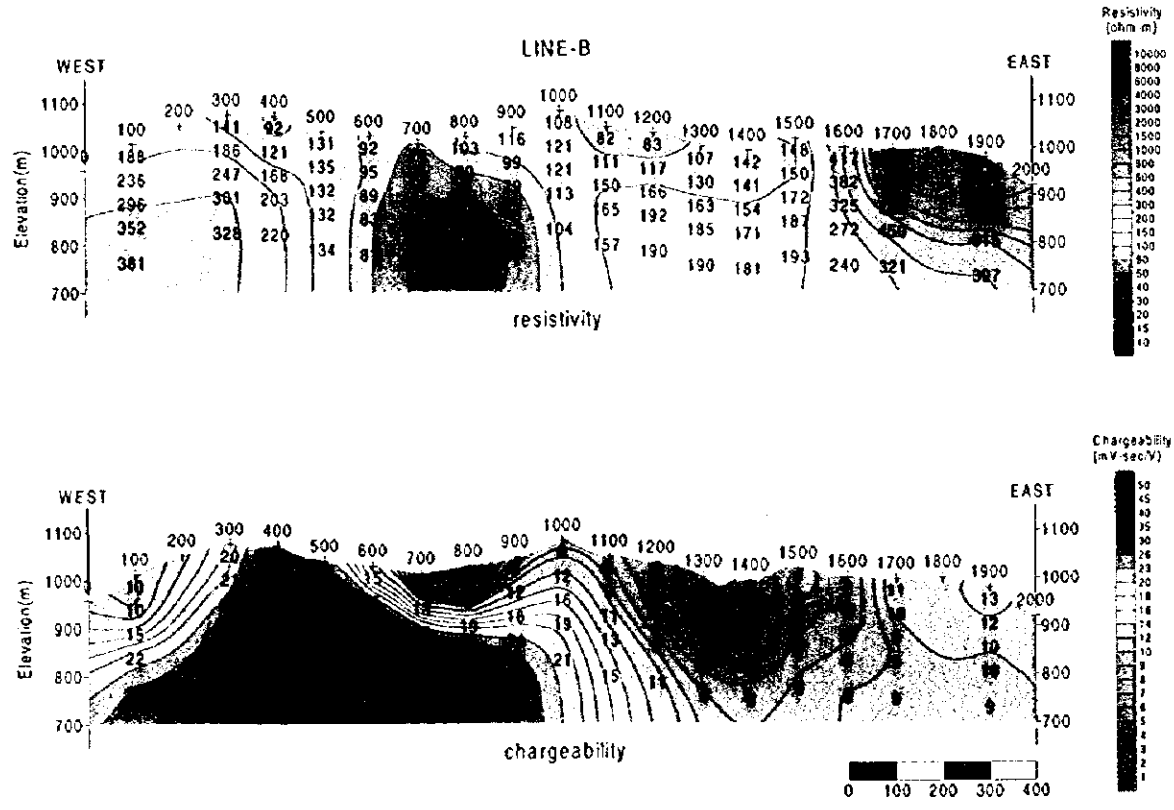

Fig.II-2-6-17 Results of model simulation of the Mae Kanai area(B)

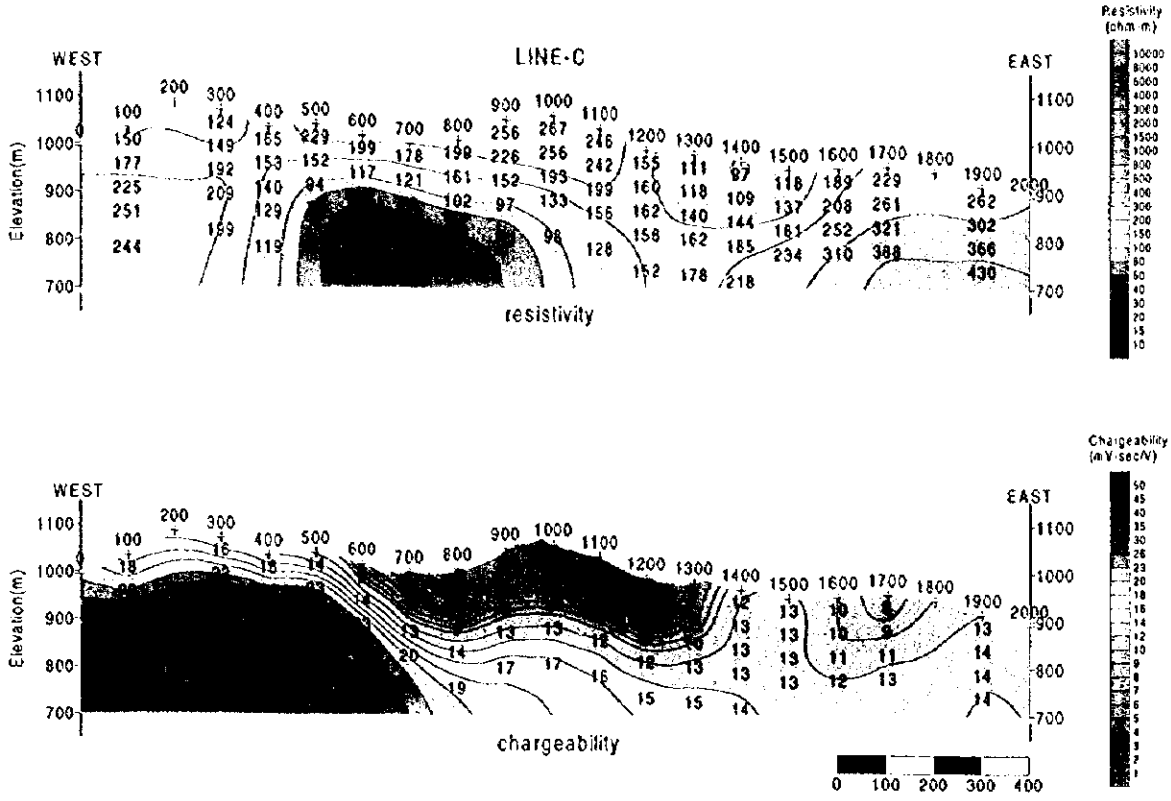

Fig.II-2-6-18 Results of model simulation of the Mae Kanai area(C)

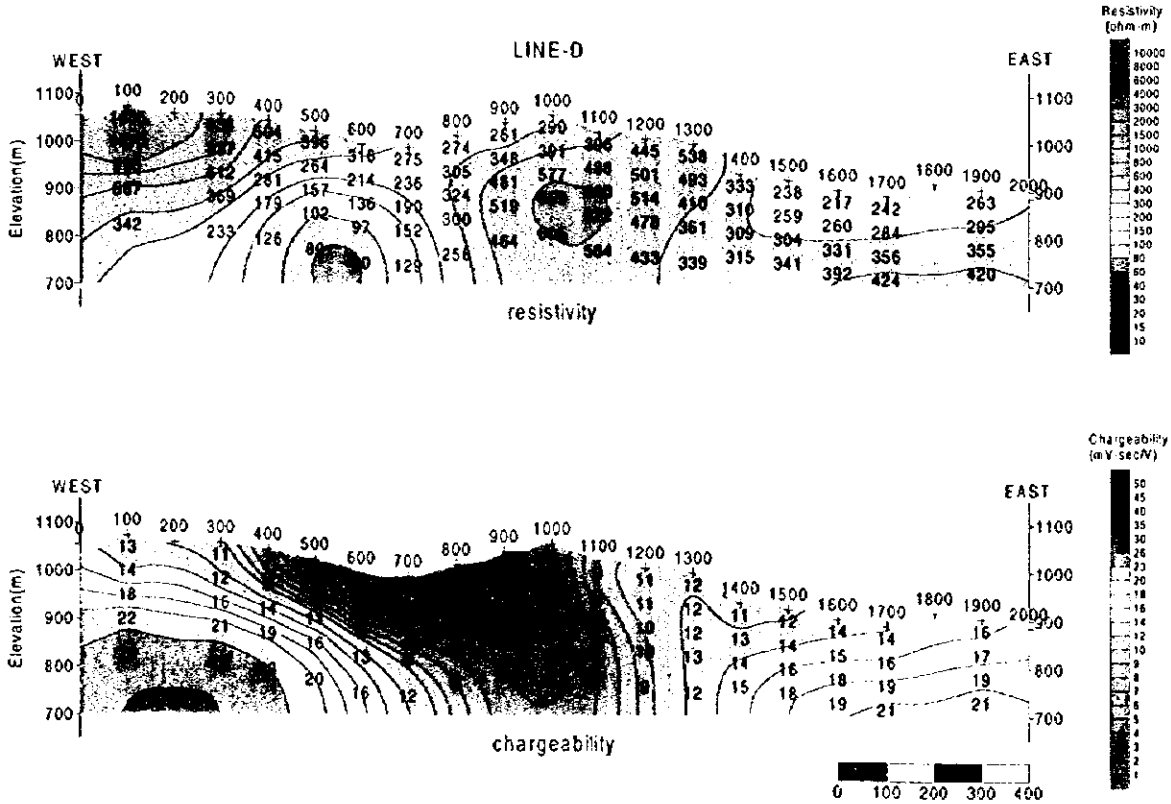

Fig.II-2-6-19 Results of model simulation of the Mae Kanai area(D)

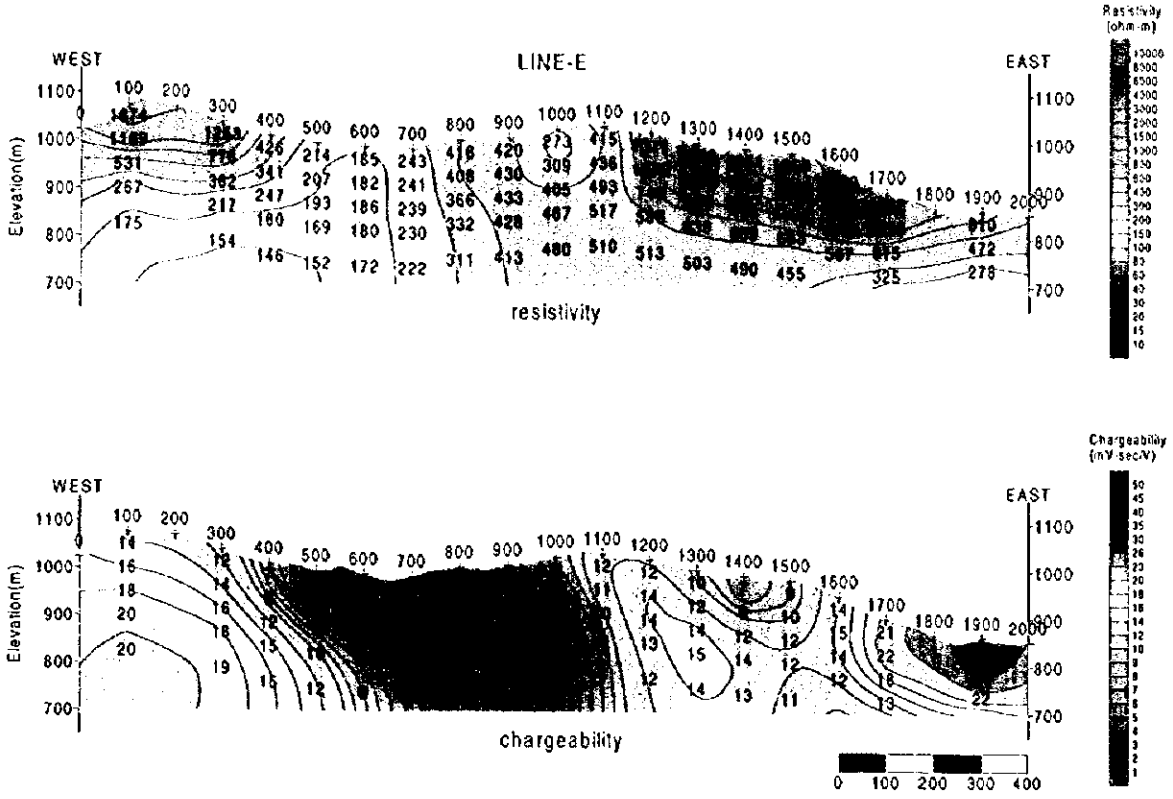

Fig.II-2-6-20 Results of model simulation of the Mae Kanai area(E)

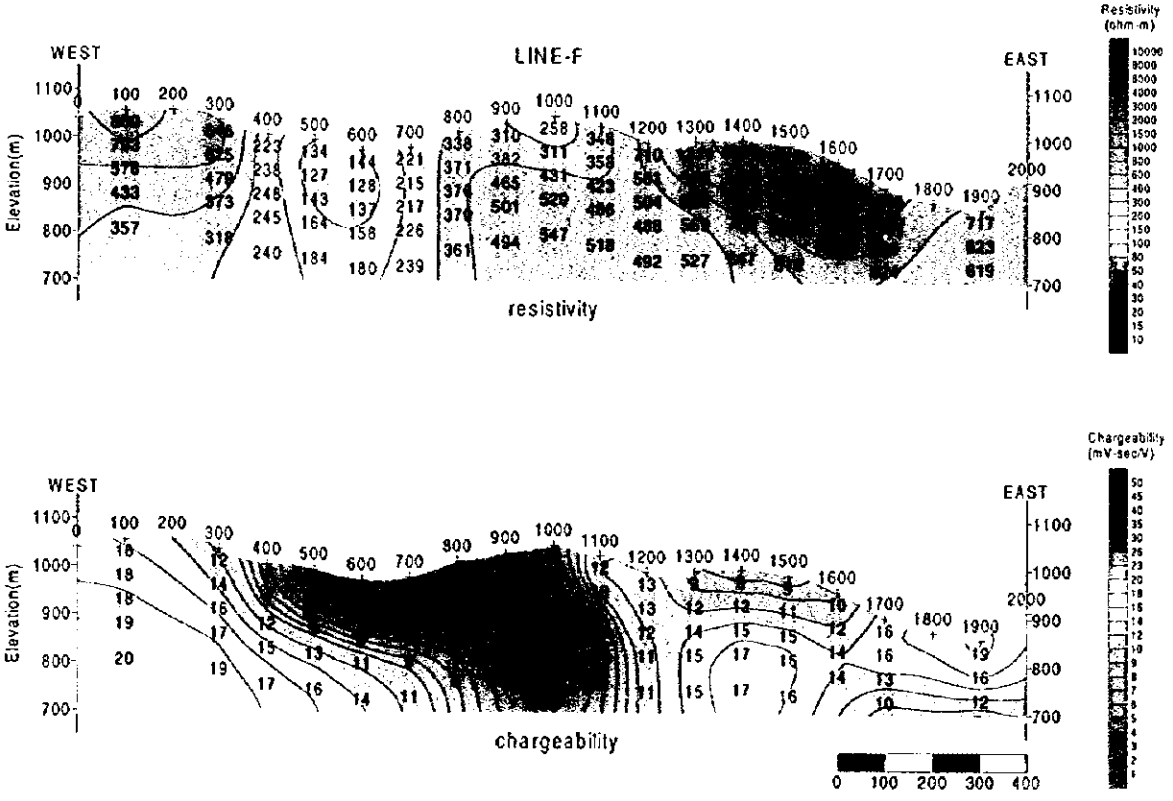

Fig.II-2-6-21 Results of model simulation of the Mae Kanai area(F)

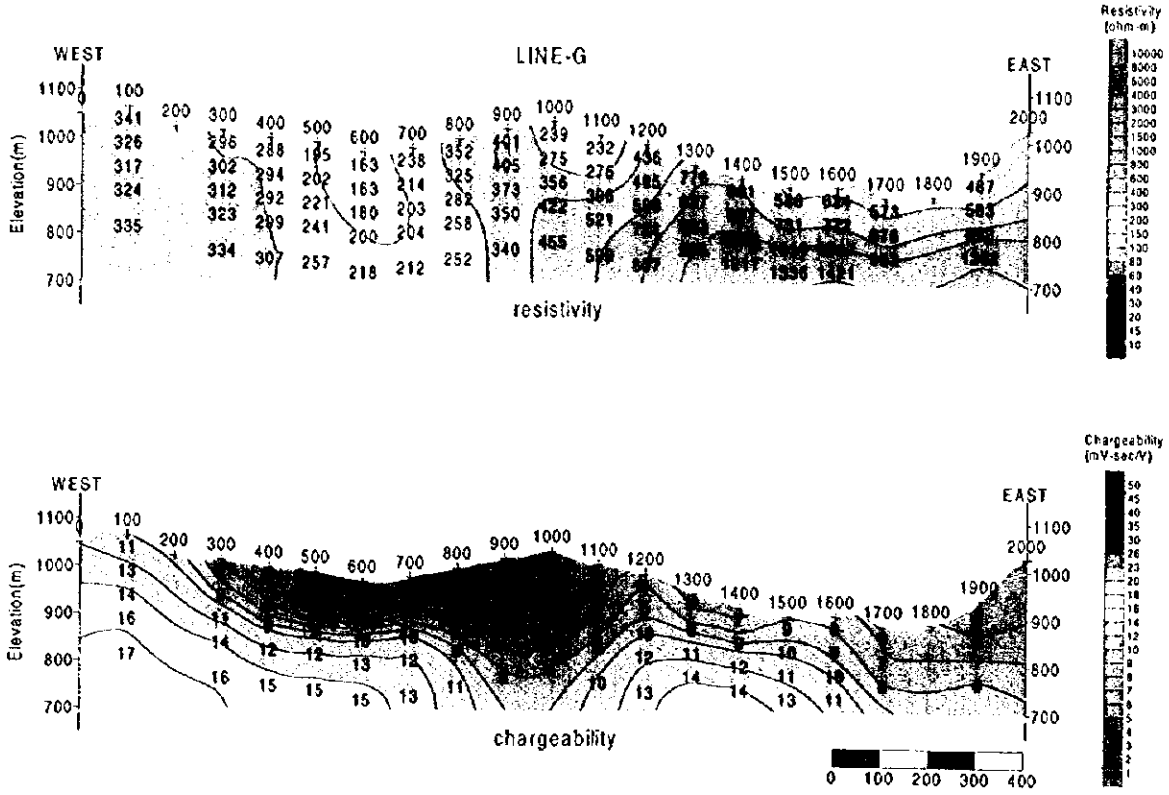

Fig.II-2-6-22 Results of model simulation of the Mae Kanai area(G)

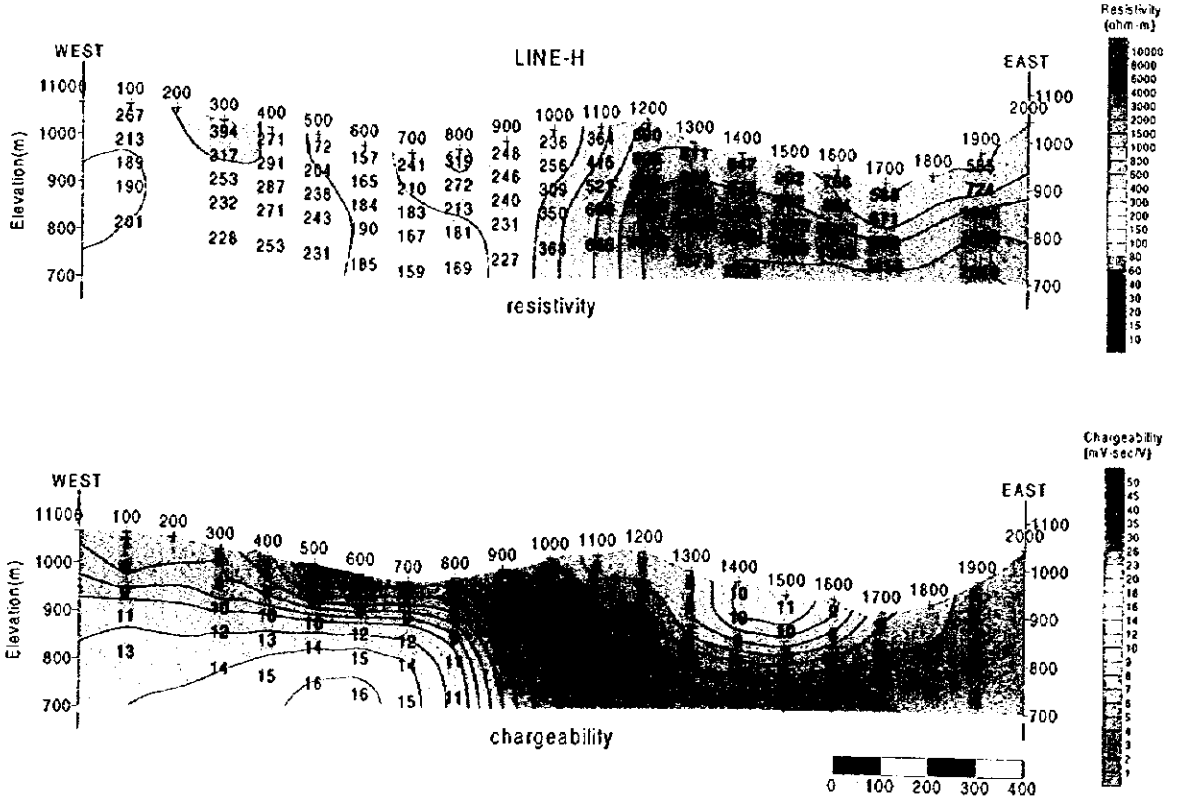

Fig.II-2-6-23 Results of model simulation of the Mae Kanai area(H)

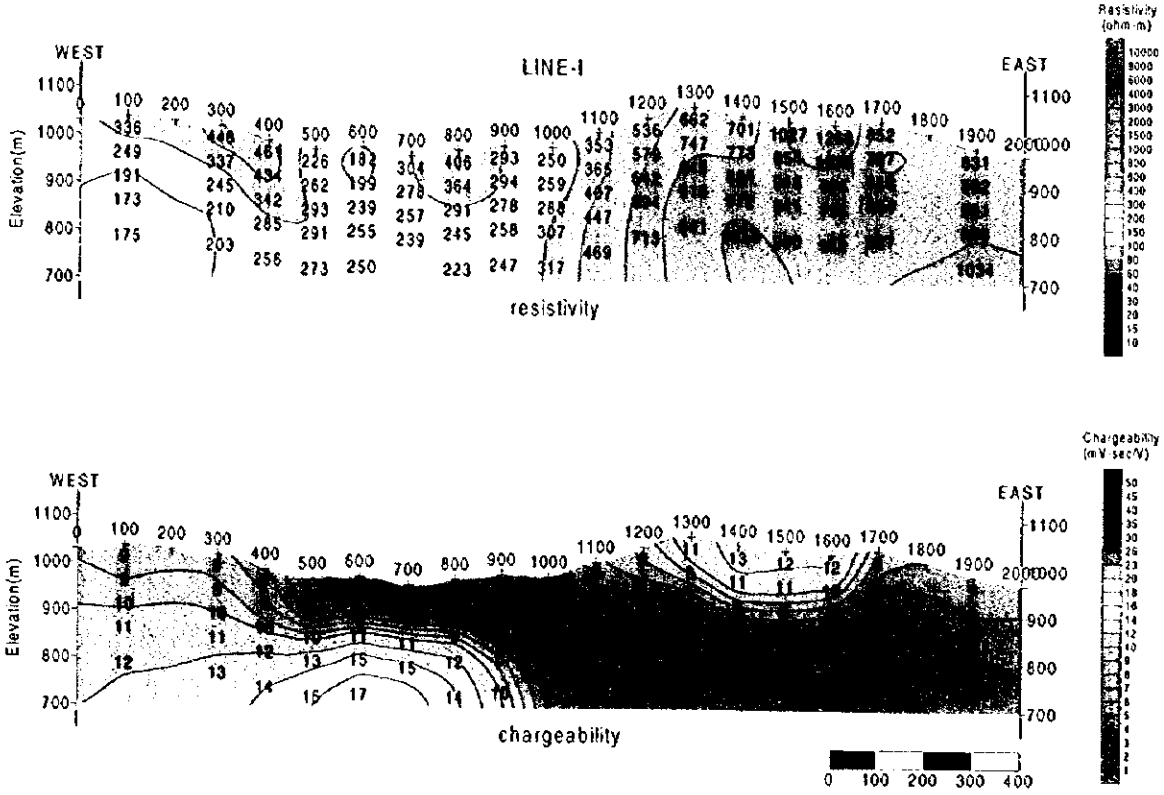

Fig.II-2-6-24 Results of model simulation of the Mae Kanai area(I)

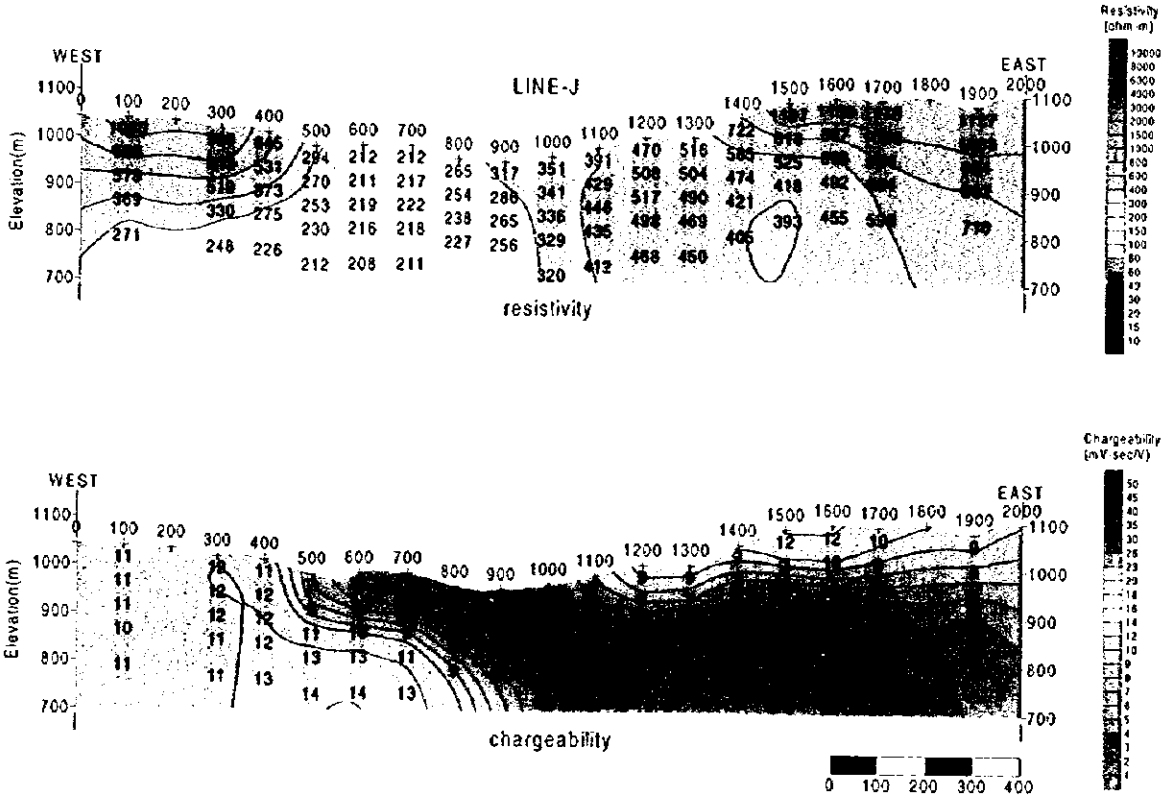

Fig.II-2-6-25 Results of model simulation of the Mae Kanai area(J)

It is assumed that the same structure is continuing to N-S direction, because the tendency of resistivity and chargeability distribution is almost same from Line H to Line J.

2-6-2-4 Consideration

The apparent resistivity of this area shows from 35 to 5186Ω·m, and the chargeability shows a maximum of 53mV·sec/V. As for the distribution of apparent resistivity, it shows different distribution from Line A to C, from Line D to J. The distribution of apparent resistivity from Line D to J show the same pattern, and the resistivity structure extends N-S direction. The low apparent resistivity distributes N-S direction, which center is station 600, and this distribution is coincident with that of alluvium in geologic map. Both sides of alluvium, shale and sandstone are distributed, and the apparent resistivity shows relatively high value. The low apparent resistivity distributes widely from Line A to C. As for the chargeability, the high value part distributes widely around station 500 of Line B. Also, the chargeability shows relatively high value at the east end of Line E.

In Fig.II-2-6-26, it is displaying the low apparent resistivity part (less than 150Ω·m), the high chargeability part (more than 15mV·sec/V) from the plan map of N=1. Also, it is displaying the faults and the mineral occurrences from the geologic map.

The low apparent resistivity distributes widely at Line A and B in the north part of survey area. This low apparent resistivity extends from station 1000 of Line B to station 1600 of Line C along the fault. The gossan occurrence is located near station 1600 of Line C. Also, the apparent resistivity shows low value from station 500 of line A to station 500 of Line C along the N-S fault. The low apparent resistivity from station 500 to station 600 of Line F are located in the alluvium, and it is supposed that there is no relation to mineralized zone.

The high chargeability zone is divided into two parts. One part is around the gossan and the N-S fault near station 300 of Line A and Line B, this high chargeability part extends to station 300 of Lime F. The mineral occurrence of magnetite is located near station 100 of Line F and this anomaly is related to this mineral occurrence, but it is located out of the survey area, then the details are obscure. The other part is from station 1800 of Line D to station 1800 of Line F, and the gossan is located around the high chargeability part, but this part is not coincident with the mineral occurrence. This high chargeability part is smaller as the depth increase. There are several small anomaly parts, but there are not coincident with the mineral occurrence.

As the result of 2-D analysis, the resistivity discontinuity is seen along the N-S fault from Line A to Line C, the low resistivity distributes at the east part of this discontinuity. The chargeability shows highest value near the station 500 of Line B, and the center of the high chargeability is shifting to the west compared with that of Line B.

As the results of these data, it is supposed that the promising part is around station 500 of Line B. In this part, the resistivity shows low value and the chargeability shows high value. Also, this part is around the fault and near the mineral occurrence, then this anomaly is related to the

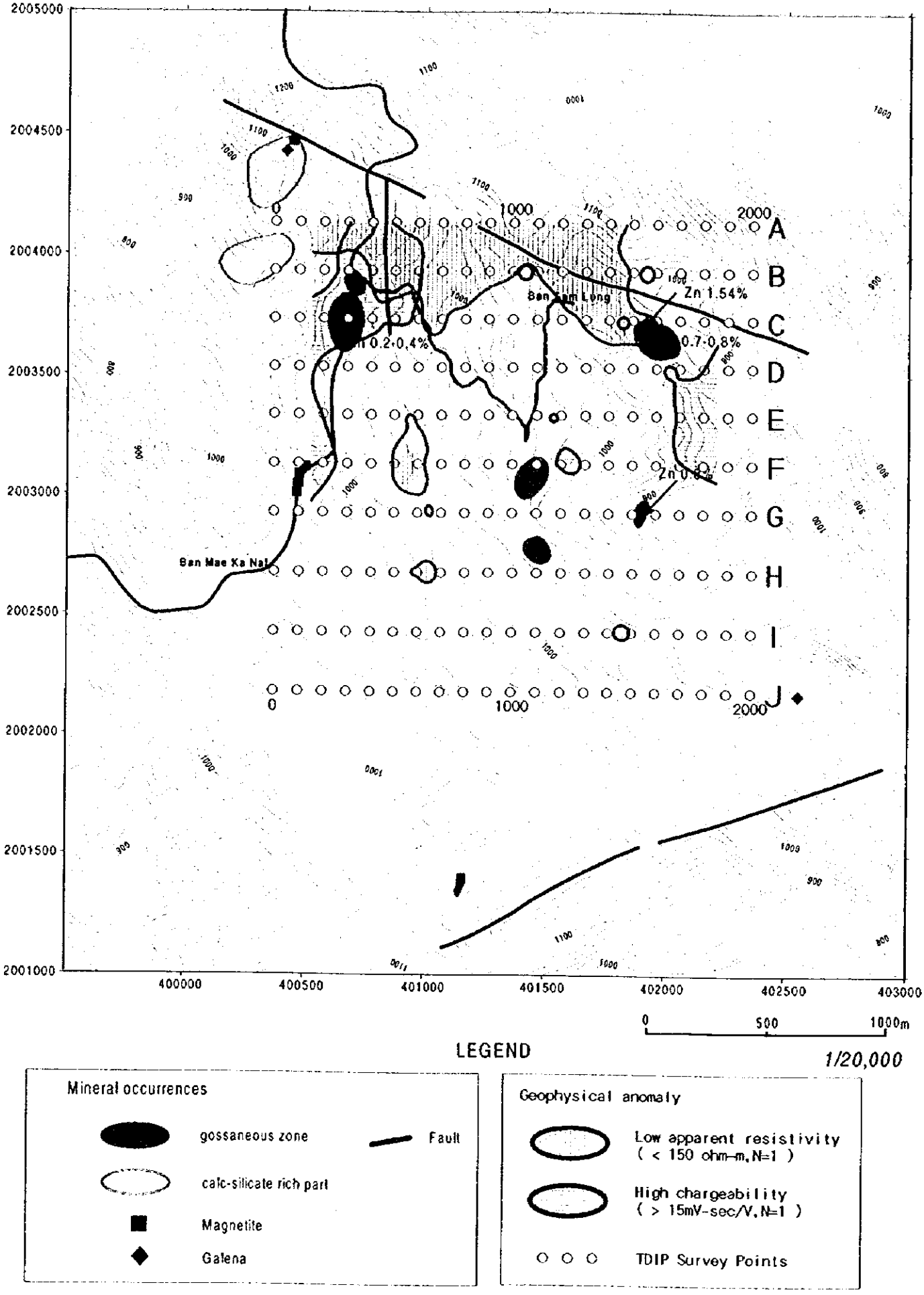

Fig. II-2-6-26 Integrated plan map of the Mae Kanai Area

mineralized zone.

2-7 General Discussion

The Mae Kanai area is underlain by the Paleozoic sedimentary rocks. Triassic granite is distributed on the west side of the sedimentary rocks.

The sedimentary rocks mainly consist of Ordovician shale, sandstone and limestone, but Silurian-Devonian sandstone is south and north, in fault contact with Ordovician rocks.

Shale and sandstone units are dominant in Ordovician rocks on the surface, but it is inferred that limestone is widely distributed under the shale and sandstone units.

More than seven gossan zones with several hundreds meters in diameter occur on the Ordovician shale and sandstone unit. They commonly contain high concentration of zinc. The gossan zone southeast of Ban Sam Lung is obtained high zinc content ranging from 0.7 to 0.8 % Zn, and maximum 1.54 % Zn. The gossan samples collected from other gossan zones are also shown high zinc content ranging from 0.2 to 0.4 % Zn on average.

Four following anomaly areas are selected on the result of the geochemical survey.

1) The area around the points ranging from 200 to 500 of Line B and Line C
2) The gossan zone southeast of Ban Sam Lung
3) The area from the F-1000 on a gossan zone to Line E
4) The periphery area around the points ranging from 800 to 900 of Line D

The highest anomaly area base on the result of the geophysical survey is a low-resistivity and high-chargeability zone around B-500 station. Its anomaly may be accompanied by a mineralization, because it is situated at a periphery of the fault zone and very near from the gossan zone.

A wide low-resistivity zone along a fault extends from B-1000 station to C-1600 station, and a high-chargeability zone extends from D-1800 station to F-1800 station. A gossan zone occurs near C-1600 station between these two IP anomaly zones. The low resistivity zone, the gossan zone and the high chargeability zone continue to the direction of the fault. Therefore it may be also accompanied by a fault-related mineralization.

The promising areas for further survey are shown as follows.

1) The area from a gossan zone to a fault, ranging from 300 to 600 stations of Line B and Line C. It overlaps with zinc anomaly, low-resistivity and IP high-chargeability zone.
2) The gossan zone and the high-chargeability zone east of Ban Sam Lung. Gossan contains high zinc content, and the zone overlaps with geochemical copper-lead-zinc MMI anomaly area. Here is also found a low-resistivity zone.

The characteristic of geochemistry and geophysical anomaly suggests that the fault-related mineralizations are expected in these areas.

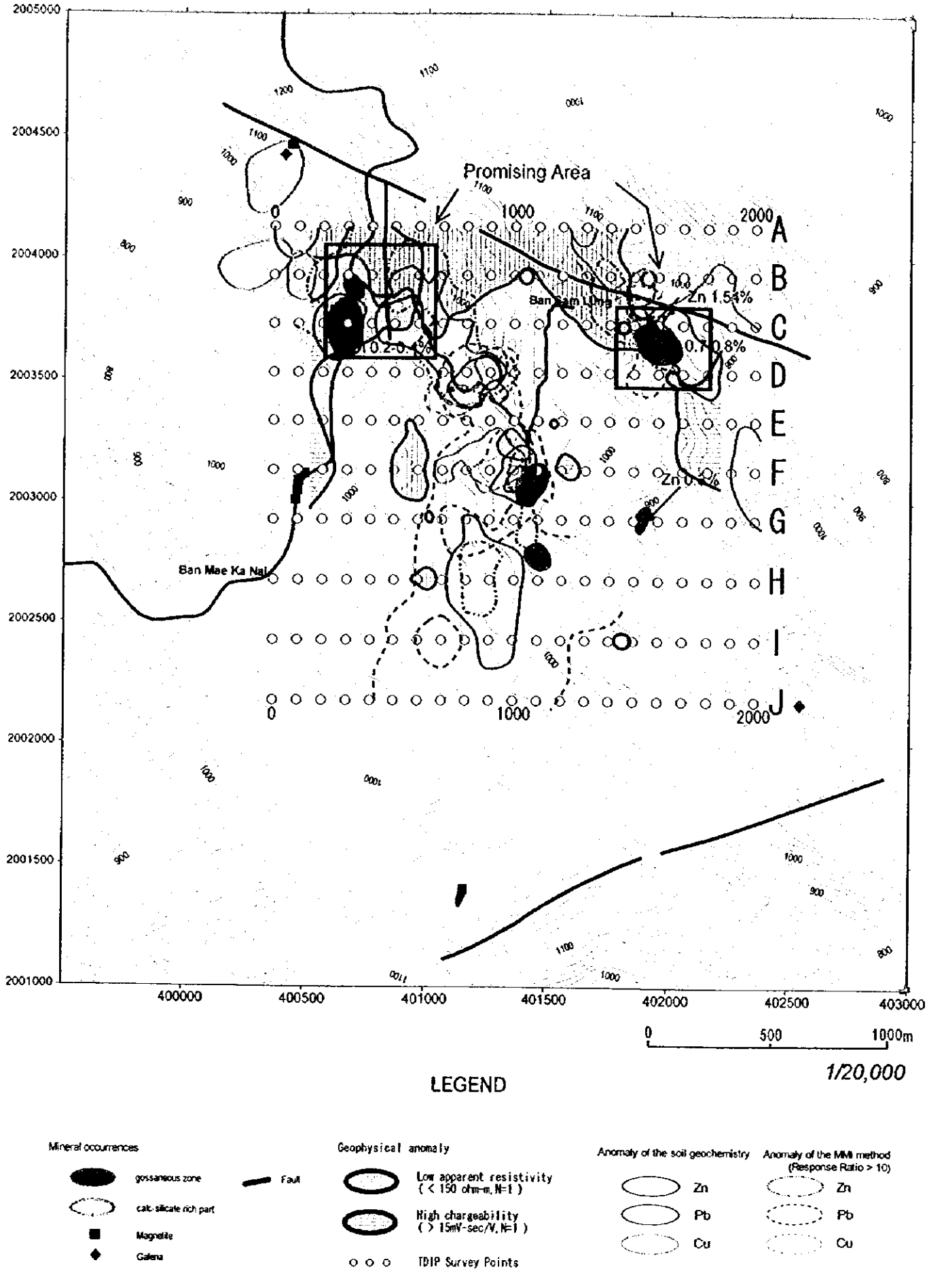

Fig. II-2-7-1 Interpretation map of the Mae Kanai Area